Analysis of an intra-and interspecific interference model with allelopathic competition *

Radhouane Fekih-Salem

Analysis of an intra- and interspecific interference model with allelopathic competition *

Radhouane Fekih-Salem†

Abstract. Understanding and exploiting competition and coexistence between microbial species is one of the more challenging aspects of mathematical biology. In this paper, we propose an original model of two-microbial species competing for a single nutrient in the chemostat including general intra- and interspecific density-dependent growth rates with allelopathic interactions. Each species produces a toxin that affects the growth of other species as well as its own growth. The removal rates are distinct and include the specific death rate and the autotoxicity of each species. We establish an in-depth mathematical analysis by determining the multiplicity of all steady states of the three-dimensional system and their necessary and sufficient conditions of existence and local stability according to the operating parameters, which are the dilution rate and the inflowing concentration of the substrate. To describe the asymptotic behavior of the process according to these control parameters, we determine the operating diagram by using the software MATCONT. The one-parameter bifurcation diagram in the dilution rate shows that there can be either transcritical or saddle-node bifurcations. We apply our results to a particular model in the literature without intra- and interspecific interference but with only allelopathic effects of the second species on the first species. We demonstrate that one of the coexistence steady states is locally exponentially stable when it exists, whereas in the literature they have not been able to demonstrate that the stability condition of this steady state is always fulfilled.

Key words. Allelopathy, bifurcation, chemostat, coexistence, density-dependence, operating diagram

MSC codes. 34A34, 34D20, 37N25, 92B05

1. Introduction.

The chemostat is an experimental device used in microbial ecology, microbiology, and evolutionary and applied biology such as water treatment, biomass energy recovery and biotechnologies in a broad sense. It is the source of several mathematical models for population dynamics and interactions between microbial species, in particular competition for resources [23, 27, 50]. The mathematical study of the classical chemostat model of several species competing on a same limiting resource shows that only the species with the lowest *break-even concentration* survives while all other species will be excluded [50]. This result is classical and is well known as the *Competitive Exclusion Principle* (CEP) which asserts that at most one species can survive to the competition, namely the species which makes optimal use of the resource (see [16] and the references therein). Hansen and Hubbell's laboratory experiments allowed to identify and validate the CEP in the chemostats [26].

However, the biodiversity and natural species richness appeared as a contradiction with the CEP. The solution to this paradox is to revise the mathematical modeling by taking into account in the classic chemostat model the different types of interactions between microbial species. Indeed, this has motivated many recent researches aimed at understanding and explaining biodiversity in microbial ecosystems by taking into account various mechanisms to

*Submitted to the editors 2023-05-16.

† University of Tunis El Manar, National Engineering School of Tunis, LAMSIN, Tunisia, and University of Monastir, Higher Institute of Computer Science of Mahdia, Tunisia (radhouane.fekih-salem@enit.utm.tn).

promote the coexistence of species. In the literature, the following coexistence mechanisms can be found: intra- and interspecific competition [1, 9], flocculation [15, 17, 18, 19, 24], density-dependence [16, 33, 34, 35, 40, 41], predator-prey interaction [2, 5, 32], simple or complex food web [6, 28, 56], presence of an internal or external inhibitors [3, 10, 11, 12, 29], and the references therein.

While these various coexistence mechanisms have been extensively analyzed with chemostat models, allelopathy is another mechanism of biodiversity between species that has been relatively neglected. Allelopathy can be defined as the effect of a toxic substance released by one species and being nocive to their own or their competitor's growth rates [37]. The applications of allelopathic competitions can be found in several fields like bio-remediation, biotechnological processes, ecological phenomena like algal blooms and so on. This kind of competition is frequent in nature not only between algal species but also between algae and bacteria, bacteria and bacteria, algae and aquatic plants, as well as plants and plants (see [21, 22], and the references therein).

Based on the formulation of phenomenological Lotka–Volterra type, allelopathic interaction modeling between two species was introduced by Maynard-Smith [39] where each species produces a toxic substance to the other but only when the other is present. An exhaustive analysis of the two-species competition model with allelopathic interactions was carried out in [7]. In order to have a good fit for all the experimental data of the toxic alga, the simple Lotka–Volterra type model with allelopathic interactions between two marine phytoplankton species was modified such that the allelopathic term depends on the product of the square of the concentration of the target species by the concentration of the toxic species [52]. More precisely, if x_1 is the population density of a non-toxic alga and x_2 that of a toxic one, the mathematical form of the allelopathic interaction term is $\alpha_1 x_1^2 x_2^2$, where α_1 is the allelopathic parameter.

Roy [45] introduced a chemostat model with two microbial species competing for a single resource by considering a single species that is toxin-producing thereby having an allelopathic effect on the other. Growth rates are specified to be of Michaelis-Menten type. An extension of Roy's competition model between non-toxic phytoplankton and toxic phytoplankton was studied in Kengwoung-Keumo [30] by allowing a general class of monotonic growth rates.

Inspired by the way to model competitions of Lotka–Volterra type by including allelopathic terms in the chemostat [30, 39, 45, 52], we propose a first general model of two species competing for a single resource in the chemostat involving an intra- and interspecific competition with allelopathic effects. Using distinct removal rates and assuming that the two populations are toxic, the model takes the form

$$\left\{\begin{array}{lcl} \dot{S} &=& D(S_{in}-S)-\mu_1(S)\frac{x_1}{y_1}-\mu_2(S)\frac{x_2}{y_2},\\ \dot{x}_1 &=& [\mu_1(S)-a_{11}x_1-a_{12}x_2-\alpha_1 x_1 x_2^2-D_1]x_1,\\ \dot{x}_2 &=& [\mu_2(S)-a_{22}x_2-a_{21}x_1-\alpha_2 x_2 x_1^2-D_2]x_2, \end{array}\right. \tag{1.1}$$

where $S(t)$ denotes the concentration of nutrient in the culture at time t; $x_1(t)$ and $x_2(t)$ denote the concentrations of the two toxic species at time t; $\mu_1(S)$ and $\mu_2(S)$ represent the per-capita growth rates of the two species; S_{in} and D denote, respectively, the input concentration of the limiting nutrient and the dilution rate of the chemostat; y_1 and y_2 are the yield coefficients which can be easily normalized to the unit without loss of generality by the simple change of

variables $x_1/y_1 \to x_1$ and $x_2/y_2 \to x_2$. In addition, a_{11} and a_{22} are the rates of intraspecific competition of the first and second species, respectively; a_{12} and a_{21} are the interspecific competition coefficients of the species j on the species i, $i = 1, 2,\ j = 1, 2,\ i \neq j$. As in Solé et al. [52], the phytotoxic (or allelopathic) interactions of the species j on the species i is modeled by $\alpha_i x_1^2 x_2^2$, where α_i denotes the phytotoxic coefficient. In addition, D_i, $i = 1, 2$, represents the disappearance rate of the species i that can be modeled as follows:

$$D_i = \theta_i D + m_i,$$

where θ_i belongs to $[0, 1]$ and denotes the proportion of the species i leaving the reactor as proposed by Bernard et al. [4] to model a biomass reactor attached to the support or to decouple the residence time of solids and the hydraulic residence time $(1/D)$. Moreover, the nonnegative mortality rate m_i of the species i is the sum of the specific death rate ϵ_i and the autotoxicity parameters a_i, that is, $m_i = \epsilon_i + a_i$ and it has unit of the dilution rate (1/day).

In this work, we propose and study a more general model than our first proposed model (1.1) by allowing generic functions representing intra- and interspecific competitions as well as toxic effects of each species on the other. This model is an extension of system (1.1) and it generalizes several models studied in the literature as we demonstrate later. This general model is written as follows:

$$\left\{\begin{array}{lcl} \dot{S} &=& D(S_{in} - S) - \mu_1(S)x_1 - \mu_2(S)x_2, \\ \dot{x}_1 &=& [\mu_1(S) - q_1(x_1, x_2) - D_1]x_1, \\ \dot{x}_2 &=& [\mu_2(S) - q_2(x_2, x_1) - D_2]x_2, \end{array}\right. \tag{1.2}$$

where the functions $q_1(x_1, x_2)$ and $q_2(x_2, x_1)$ are assumed to be decreasing in each variable x_1 and x_2.

The particular case of our general model (1.2) was considered in [45] when the growth rates $\mu_1(S)$ and $\mu_2(S)$ are of Michaelis-Menten type and when only the first species produces toxin, that is, $q_2(x_2, x_1) = 0$. The author has derived analytically a critical lower bound of allelopathy as a function of the parameters of model which ensures the coexistence and the coevolution of two phytoplankton species competing for a single limiting nutrient. The local stability of positive steady states has been determined only numerically. Using a general class of monotonic growth rates, an extension of model [45] has been studied in [30]. The author has shown the existence of two interior steady states where the stability of one of them depends on a condition of Routh–Hurwitz criterion. In this work, we will show that this condition is always satisfied in their particular case.

In Fekih-Salem et al. [20], we have considered only the interspecific interactions in the dynamics of the first species, that is, $q_1(x_1, x_2) = q_1(x_2)$ and $q_2(x_2, x_1) = 0$. We have shown the occurrence of positive steady state of coexistence but which is unstable as long as it exists. Then, taking into account the intra- and interspecific interference such that $q_1(x_1, x_2) = q_1(x_2)$ and $q_2(x_2, x_1) = q_2(x_2)$, there can be a multiplicity of positive steady states which could be locally exponentially stable.

Note that the structure of our model (1.2) is different from that in our paper Fekih-Salem et al. [16]. In fact, here we consider the growth rates $\mu_1(S)$ and $\mu_2(S)$ (which depend only on S) in the dynamics of the substrate S. However, in [16], it is rather the density-dependent

growth rates $\mu_1(S, x_1, x_2)$ and $\mu_2(S, x_1, x_2)$ (which depend only on S, x_1, and x_2) in the dynamics of S.

The aim of this paper is to provide a complete mathematical and numerical analysis of the general model (1.2) to understand the joint effect of the intra- and interspecific density-dependence with allelopathic competitions. Our study presents an extension of the results in [30, 45] by allowing a general class of growth functions and the production of both species of the toxin and by adding the intra- and interspecific interference. Using distinct removal rates including mortality and autotoxicity of each species, we describe the multiplicity of all steady states and their necessary and sufficient conditions of existence and local stability according to the operating parameters S_{in} and D. To determine the asymptotic behavior of the process with respect to these two operating parameters, we analyze the operating diagram using the software MATCONT. To describe all types of bifurcations, we study the one-parameter bifurcation diagram in D. Then, we apply our theoretical results to the particular model (6.1) of [30] by providing the necessary and sufficient conditions of existence and local stability of all steady states. In particular, we prove that one of the two positive steady states is locally exponentially stable when it exists, whereas in [30] the author has not been able to demonstrate that the stability condition of this steady state is always fulfilled. In this particular case of [30], we determine theoretically the operating diagram and the one-parameter bifurcation diagram which have not been studied in the literature. Finally, the numerical simulations illustrate the theoretical results.

This paper is organized as follows. The next section presents general assumptions for the density-dependent functions of model (1.2). Subsequently, we show mathematically that it is biologically well-posed and we study of the existence of all steady states and their multiplicity. Section 3 is devoted to the analysis of the local asymptotic stability of each steady state of system (1.2). Using the software MATCONT [38], the operating diagram is established in section 4 according to S_{in} and D as the bifurcation parameters. In section 5, the one-parameter bifurcation diagram in the dilution rate D illustrates all types of bifurcations. In section 6, our results are applied to the particular model (6.1) of [30]. In section 7, we discuss and compare our results with the results of the existing literature. In Appendix A, we show that one of the stability conditions of the Routh–Hurwitz criterion corresponding to the coexistence steady states holds for all S_{in} and D. Finally, all parameter values used in the numerical simulations are provided in Appendix B.

2. Assumptions on the model and steady states. In this work, we assume that the growth rates of model (1.2) are continuously differentiable ($\mathcal{C}^1$) functions that satisfy the following general conditions.

Hypothesis 2.1. $\mu_1(0) = \mu_2(0) = 0$ and $\mu_1'(S) > 0$ and $\mu_2'(S) > 0$, for all $S > 0$.

Hypothesis 2.1 means that the growth can take place if and only if the substrate is present and the growth rate of each species increases with the concentration of substrate.

Hypothesis 2.2. $q_1(0,0) = q_2(0,0) = 0$, $q_1(x_1, x_2) \geq 0$, $q_2(x_2, x_1) \geq 0$, $\frac{\partial q_1}{\partial x_1}(x_1, x_2) \geq 0$, $\frac{\partial q_1}{\partial x_2}(x_1, x_2) \geq 0$, $\frac{\partial q_2}{\partial x_2}(x_2, x_1) \geq 0$ and $\frac{\partial q_2}{\partial x_1}(x_2, x_1) \geq 0$, for all $x_1 > 0$ and $x_2 > 0$.

The negative effects of intra- and interspecific interference and allelopathic competition increase with the concentration of species x_1 and x_2.

The following preliminary result shows the positivity and boundedness of the solutions of model (1.2) which are very important properties for any biological and ecological system. The proof is standard and hence is left to the reader.

Proposition 2.3. *For any nonnegative initial condition, the solutions of model (1.2) remain nonnegative and are positively bounded. Let* $D_{\min} = \min(D, D_1, D_2)$. *The compact set*

$$\Omega = \left\{ (S, x_1, x_2) \in \mathbb{R}^3_+ : S + x_1 + x_2 \leq \frac{D}{D_{\min}} S_{in} \right\},$$

is positively invariant and is a global attractor for system (1.2).

The steady states are found by setting the right hand sides of equations of (1.2) equal to zero. Thus, they are the solutions of the set of equations

$$\left\{ \begin{array}{rcl} 0 & = & D(S_{in} - S) - \mu_1(S)x_1 - \mu_2(S)x_2, \\ 0 & = & [\mu_1(S) - q_1(x_1, x_2) - D_1]x_1, \\ 0 & = & [\mu_2(S) - q_2(x_2, x_1) - D_2]x_2. \end{array} \right. \tag{2.1}$$

Indeed, system (1.2) can have at most four types of steady states labeled as follows:

- $\mathcal{E}_0 = (S_{in}, 0, 0)$: the washout of both species ($x_1 = x_2 = 0$). It always exists.
- $\mathcal{E}_1 = (\tilde{S}_1, \tilde{x}_1, 0)$: only the second species is extinct ($x_2 = 0$ and $\tilde{x}_1 > 0$).
- $\mathcal{E}_2 = (\tilde{S}_2, 0, \tilde{x}_2)$: only the first species is extinct ($x_1 = 0$ and $\tilde{x}_2 > 0$).
- $\mathcal{E}^* = (S^*, x_1^*, x_2^*)$: both species are maintained ($x_1^* > 0$ and $x_2^* > 0$).

From Hypothesis 2.1, when equation $\mu_i(S) = D_i$, $i = 1, 2$ has a solution, it is unique and we define the usual *break-even concentrations*

$$\lambda_i = \mu_i^{-1}(D_i). \tag{2.2}$$

When equation $\mu_i(S) = D_i$ has no solution, we put $\lambda_i = +\infty$.

The following result determines the components and the uniqueness of the boundary steady states $\mathcal{E}_1$ and $\mathcal{E}_2$, as well as their existence conditions according to the operating parameters.

Proposition 2.4. *Assume that Hypotheses 2.1 and 2.2 hold. The boundary steady states* $\mathcal{E}_1 = (\tilde{S}_1, \tilde{x}_1, 0)$ *and* $\mathcal{E}_2 = (\tilde{S}_2, 0, \tilde{x}_2)$ *of system (1.2) are defined by*

$$\tilde{S}_i = \varphi_i(\tilde{x}_i) := S_{in} - \frac{D_i}{D}\tilde{x}_i - \frac{1}{D} q_i(\tilde{x}_i, 0)\tilde{x}_i, \quad i = 1, 2 \tag{2.3}$$

and $\tilde{x}_i$ *is the unique solution of equation*

$$\psi_i(x_i) := \mu_i(\varphi_i(x_i)) - q_i(x_i, 0) - D_i. \tag{2.4}$$

$\mathcal{E}_i$ *exists if and only if* $S_{in} > \lambda_i(D)$. *When it exists,* $\mathcal{E}_i$ *is unique.*

Proof. Let $i = 1, 2$, $j = 1, 2$, $i \neq j$. The components $S = \tilde{S}_i$ and $x = \tilde{x}_i$ of a boundary steady state $\mathcal{E}_i$ are the solutions of (2.1) with $x_i > 0$ and $x_j = 0$. Thus, $\tilde{S}_i$ and $\tilde{x}_i$ are the solutions of equations

$$\left\{ \begin{array}{rcl} D(S_{in} - S) & = & \mu_i(S)x_i, \\ \mu_i(S) & = & q_i(x_i, 0) + D_i. \end{array} \right. \tag{2.5}$$

Using the two equations of (2.5), it follows that $S = \varphi_i(x_i)$ which is defined in (2.3). Replacing this expression of S in the second equation of (2.5), we see that x_i must be a solution of the equation $\psi_i(x_i) = 0$. The derivative of $\varphi_i(x_i)$ is given by

$$\varphi_i'(x_i) = -\frac{1}{D}\left(q_i(x_i,0) + \frac{\partial q_i}{\partial x_i}(x_i,0)x_i + D_i\right).$$

From Hypothesis 2.2, the mapping $x_i \mapsto \varphi_i(x_i)$ is monotonically decreasing from $\varphi_i(0) = S_{in}$ to

$$\varphi_i\left(\frac{D}{D_i}S_{in}\right) = -\frac{S_{in}}{D_i}q_i\left(\frac{D}{D_i}S_{in}, 0\right) \leq 0.$$

Hence, there exists a unique solution $\hat{x}_i \in (0, DS_{in}/D_i]$ satisfying $\varphi_i(x_i) = 0$. In addition, $S = \varphi_i(x_i)$ is nonnegative for all $x_i \leq \hat{x}_i$. On the other hand, we have

$$\psi_i'(x_i) = \varphi_i'(x_i)\mu_i'(\varphi_i(x_i)) - \frac{\partial q_i}{\partial x_i}(x_i,0).$$

From Hypotheses 2.1 and 2.2, the mapping $x_i \mapsto \psi_i(x_i)$ is monotonically decreasing from $\psi_i(0) = \mu_i(S_{in}) - D_i$ to $\psi_i(\hat{x}_i) = -q_i(\hat{x}_i, 0) - D_i < 0$. Therefore, there exists a unique solution $\tilde{x}_i \in (0, \hat{x}_i)$ of equation $\psi_i(x_i) = 0$ if and only if $\mu_i(S_{in}) > D_i$, that is, $S_{in} > \lambda_i$. ∎

Now, to establish the existence of the positive steady state $\mathcal{E}^* = (S^*, x_1^*, x_2^*)$, we need to show the following results. In fact, the components $S = S^*$, $x_1 = x_1^*$ and $x_2 = x_2^*$ of $\mathcal{E}^*$ must be the solutions of (2.1) with $x_1 > 0$ and $x_2 > 0$. Thus, S^*, x_1^* and x_2^* are the solutions of the set of equations

$$\left\{\begin{array}{rcl} D(S_{in} - S) & = & \mu_1(S)x_1 + \mu_2(S)x_2, \\ \mu_1(S) & = & q_1(x_1, x_2) + D_1, \\ \mu_2(S) & = & q_2(x_2, x_1) + D_2. \end{array}\right. \tag{2.6}$$

Multiplying the second equation by x_1 and the third equation by x_2 in system (2.6), the first equation implies that

$$S = S_{in} - g(x_1, x_2), \quad \text{where} \quad g(x_1, x_2) := \frac{1}{D}(D_1x_1 + x_1q_1(x_1, x_2) + D_2x_2 + x_2q_2(x_2, x_1)). \tag{2.7}$$

Consider now replacing of S by this expression (2.7) in the second and third equations of (2.6) to see that $(x_1 = x_1^*, x_2 = x_2^*)$ must be a solution of the set of equations

$$\left\{\begin{array}{rcl} 0 & = & f_1(x_1, x_2) := \mu_1(S_{in} - g(x_1, x_2)) - q_1(x_1, x_2) - D_1, \\ 0 & = & f_2(x_2, x_1) := \mu_2(S_{in} - g(x_1, x_2)) - q_2(x_2, x_1) - D_2. \end{array}\right. \tag{2.8}$$

Note that the functions f_1 and f_2 are defined on the set

$$\Lambda = \{(x_1, x_2) \in \mathbb{R}_+ \times \mathbb{R}_+ : \quad g(x_1, x_2) \leq S_{in}\}. \tag{2.9}$$

The components of the positive steady state $\mathcal{E}^*$ are positive if and only if system (2.8) has a solution in Λ°, the interior of Λ. To solve system (2.8) in the open set Λ°, we define the function corresponding to equation $S_{in} = g(x_1, x_2)$ in the following lemma.

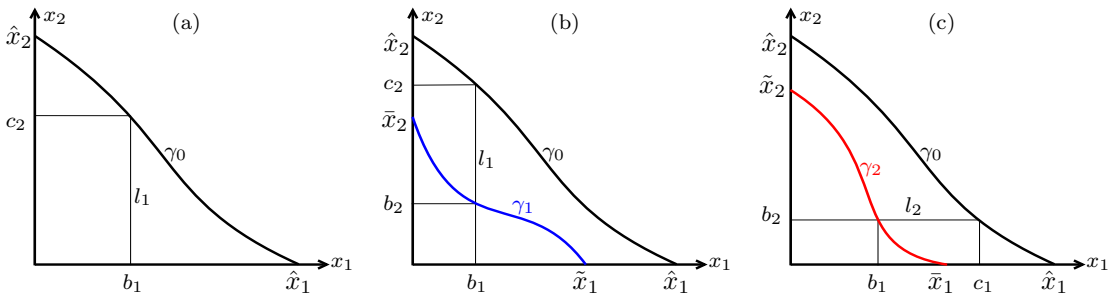

Figure 1. *(a-b-c) Definitions of the functions $x_2 = G(x_1)$, $x_2 = F_1(x_1)$ and $x_1 = F_2(x_2)$, and the corresponding graphs γ_0, γ_1 and γ_2 (in black, blue and red), respectively.*

Lemma 2.5. *Under Hypothesis 2.2, the equation $S_{in} = g(x_1, 0)$ [resp. $S_{in} = g(0, x_2)$] has a unique positive solution $\hat{x}_1 \in (0, DS_{in}/D_1]$ [resp. $\hat{x}_2 \in (0, DS_{in}/D_2]$]. Moreover, the equation $S_{in} = g(x_1, x_2)$ defines a smooth decreasing function*

$$G : [0, \hat{x}_1] \to [0, \hat{x}_2], \quad x_1 \mapsto G(x_1) = x_2$$

where $G(\hat{x}_1) = 0$ and $G(0) = \hat{x}_2$ (see Figure 1).

Proof. From proof of Proposition 2.4, there exists a unique solution $\hat{x}_i \in (0, DS_{in}/D_i]$, for $i = 1, 2$ satisfying $\varphi_i(x_i) = 0$ which is equivalent to $S_{in} = g(x_1, 0)$ and $S_{in} = g(0, x_2)$, respectively. This proves the first assertion of the lemma.

Let l_1 be the fixed line defined by $x_1 = b_1$ (see Figure 1(a)). To prove the second assertion of the lemma, we must show that each line l_1 intersects the set $S_{in} = g(x_1, x_2)$ once if and only if $0 \le b_1 \le \hat{x}_1$. From Hypothesis 2.2, the function $x_2 \mapsto S_{in} - g(b_1, x_2)$ is decreasing from $S_{in} - g(b_1, 0)$ for $x_2 = 0$ to $S_{in} - g(b_1, \hat{x}_2)$ for $x_2 = \hat{x}_2$. Since $S_{in} = g(0, \hat{x}_2)$ and the function $x_1 \mapsto g(x_1, \hat{x}_2)$ is increasing, then $g(0, \hat{x}_2) - g(b_1, \hat{x}_2) \le 0$. Consequently, there exists a unique solution $c_2 \in [0, \hat{x}_2]$ of equation $S_{in} = g(b_1, x_2)$ if and only if

$$S_{in} - g(b_1, 0) \ge 0 = S_{in} - g(\hat{x}_1, 0)$$

or (equivalently) $b_1 \le \hat{x}_1$ as the function $x_1 \mapsto S_{in} - g(x_1, 0)$ is decreasing. Thus, there exists a unique $c_2 \in [0, \hat{x}_2]$ solution of equation $S_{in} = g(b_1, x_2)$, for all $b_1 \in [0, \hat{x}_1]$. Define the function G by $c_2 = G(b_1)$. That this function G is smooth and decreasing follows from the implicit function theorem. In fact, under Hypothesis 2.2, the sign of the partial derivatives of g can be determined by

$$G_i := \frac{\partial g}{\partial x_i}(x_1, x_2) = \frac{1}{D}(D_i + q_i + x_i Q_{ii} + x_j Q_{ji}), \tag{2.10}$$

which is positive for $i = 1, 2$, $j = 1, 2$, $i \ne j$ since Q_{1i} and Q_{2i} are positive and defined by

$$Q_{1i} = \frac{\partial q_1}{\partial x_i}(x_1, x_2), \quad Q_{2i} = \frac{\partial q_2}{\partial x_i}(x_2, x_1). \tag{2.11}$$

Hence, the function G is smooth and its derivative is

$$G'(x_1) = -\frac{\frac{\partial g}{\partial x_1}(x_1, x_2)}{\frac{\partial g}{\partial x_2}(x_1, x_2)} = -\frac{G_1}{G_2} = -\frac{D_1 + q_1(x_1, x_2) + x_1 Q_{11} + x_2 Q_{21}}{D_2 + q_2(x_2, x_1) + x_2 Q_{22} + x_1 Q_{12}}.$$

It follows that G is decreasing since all terms in this fraction are positive. ∎

Proposition 2.6. *Assume that Hypotheses 2.1 and 2.2 hold. Let $S_{in} > \lambda_i(D)$, $i = 1, 2$. For $j = 1, 2$, $i \neq j$, the equation $f_i(x_i, x_j) = 0$ defines a smooth decreasing function*

$$F_i : [0, \tilde{x}_i] \to [0, \bar{x}_j], \quad x_i \mapsto F_i(x_i) = x_j,$$

where $F_i(\tilde{x}_i) = 0$ and $F_i(0) = \bar{x}_j$ so that the graph γ_i of F_i lies in Λ°, the interior of Λ defined in (2.9) (see Figure 1). Indeed, $(x_1, F_1(x_1)) \in \Lambda^\circ$ [resp. $(F_2(x_2), x_2) \in \Lambda^\circ$], for all $x_1 \in (0, \tilde{x}_1)$ [resp. $x_2 \in (0, \tilde{x}_2)$]. The derivative of F_i is given by

$$F_i'(x_i) = -\frac{E_i G_i + Q_{ii}}{E_i G_j + Q_{ij}} < 0, \quad \text{for all} \quad x_i \in [0, \tilde{x}_i], \quad \text{where} \tag{2.12}$$

$$E_i := \mu_i'(S) = \mu_i'(S_{in} - g(x_1, x_2)). \tag{2.13}$$

Proof. To facilitate understanding, we choose $i = 1$ and $j = 2$. But the case $i = 2$ and $j = 1$ can be treated similarly using the symmetry of system (2.8). Let l_1 be the fixed line defined by $x_1 = b_1$. It suffices to show that that each line l_1 intersects the set $f_1(x_1, x_2) = 0$ once if and only if $0 \leq b_1 \leq \tilde{x}_1$ so that the intersection belongs to Λ° (see Figure 1(b)). From Lemma 2.5, the curve γ_0 of the function $x_2 = G(x_1)$ intersects the line l_1 at the point $x_2 = c_2$ where

$$c_2 = G(b_1) \quad \text{or equivalently} \quad S_{in} = g(b_1, c_2).$$

From Hypotheses 2.1 and 2.2, the function $x_2 \mapsto \mu_1(S_{in} - g(b_1, x_2)) - D_1 - q_1(b_1, x_2)$ is decreasing from $\mu_1(S_{in} - g(b_1, 0)) - D_1 - q_1(b_1, 0)$ for $x_2 = 0$ to $-D_1 - q_1(b_1, c_2)$ for $x_2 = c_2$. As $-D_1 - q_1(b_1, c_2)$ is negative, then there exists a unique solution $b_2 \in [0, c_2)$ of equation $f_1(b_1, x_2) = 0$ if and only if

$$\mu_1(S_{in} - g(b_1, 0)) - D_1 - q_1(b_1, 0) \geq 0 = \mu_1(S_{in} - g(\tilde{x}_1, 0)) - D_1 - q_1(\tilde{x}_1, 0).$$

Since the function $x_1 \mapsto \psi_1(x_1)$ defined by (2.4) is decreasing, this last condition is equivalent to $b_1 \leq \tilde{x}_1$. Hence, there exists a unique solution $b_2 \in [0, c_2)$ of equation $f_1(b_1, x_2) = 0$ for all $b_1 \in [0, \tilde{x}_1]$. Define the function F_1 by $b_2 = F_1(b_1)$ where $F_1(\tilde{x}_1) = 0$ and $F_1(0) = \bar{x}_2$ which are the solutions of $f_1(\tilde{x}_1, 0) = 0$ and $f_1(0, \bar{x}_2) = 0$. That this function F_1 is smooth and decreasing follows from the implicit function theorem. Indeed, under Hypothesis 2.2, the sign of the partial derivatives of f_1 can be determined by

$$\frac{\partial f_1}{\partial x_1}(x_1, x_2) = -(E_1 G_1 + Q_{11}), \quad \frac{\partial f_1}{\partial x_2}(x_1, x_2) = -(E_1 G_2 + Q_{12}),$$

where E_1, G_1, G_2, Q_{11} and Q_{12} are positive and defined in (2.10), (2.11), and (2.13). Consequently, we obtain the function F_1' defined in (2.12) which is negative so that the function F_1 is smooth and decreasing. ∎

Proposition 2.7. *System (1.2) has a positive steady state $\mathcal{E}^* = (S^*, x_1^*, x_2^*)$ if and only if the curves γ_1 and γ_2 have a positive intersection such that the coordinates (x_1^*, x_2^*) are the positive solutions of equations*

$$x_2 = F_1(x_1) \quad \text{and} \quad x_1 = F_2(x_2), \tag{2.14}$$

with $S^* = S_{in} - g(x_1^*, x_2^*)$ where the function g is defined in (2.7).

Proof. A positive steady state $\mathcal{E}^*$ of (1.2) exists if and only if the equations $f_1(x_1, x_2) = 0$ and $f_2(x_2, x_1) = 0$ has a solution in Λ° which is the interior of Λ defined by (2.9). Using Proposition 2.6, it exists if and only if the curves γ_1 and γ_2 have a positive intersection (x_1^*, x_2^*) such that (2.14) holds where the expression of S^* is given by (2.7). ∎

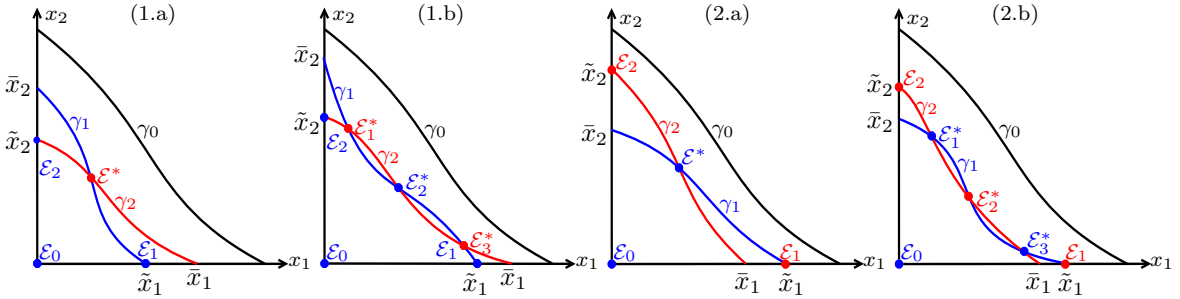

Figure 2. *Case 1 : $\bar{x}_1 > \tilde{x}_1$ and $\bar{x}_2 > \tilde{x}_2$; Case 2 : $\bar{x}_1 < \tilde{x}_1$ and $\bar{x}_2 < \tilde{x}_2$: (a) unique intersection, (b) an odd number of intersections.*

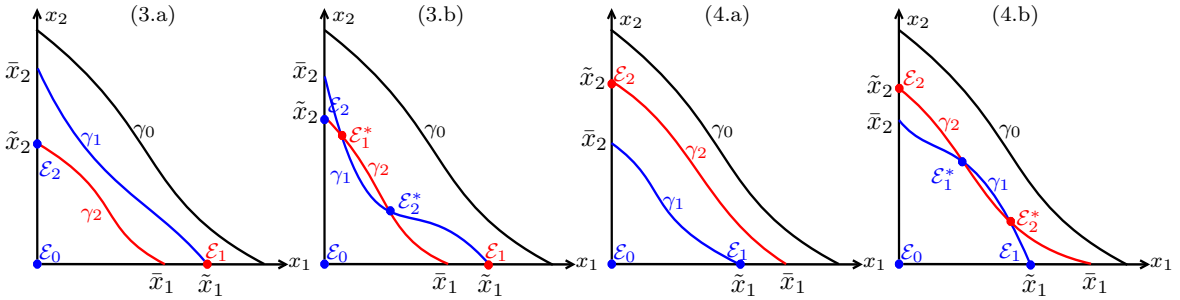

Figure 3. *Case 3 : $\bar{x}_1 < \tilde{x}_1$ and $\bar{x}_2 > \tilde{x}_2$; Case 4 : $\bar{x}_1 > \tilde{x}_1$ and $\bar{x}_2 < \tilde{x}_2$: (a) no intersection, (b) an even number of intersections.*

Note that $\tilde{x}_1$, $\tilde{x}_2$, $\bar{x}_1$ and $\bar{x}_2$ represent the coordinates of the intersections of the curves γ_1 and γ_2 with the x_1 and the x_2 axes. According to the relative positions of these values, the four cases that must be distinguished are summarized in Table 1.

Table 1

Classification of the values of $\bar{x}_i$ and $\tilde{x}_i$ to four cases for $i = 1, 2$.

Case	$\bar{x}_1$, $\tilde{x}_1$	$\bar{x}_2$, $\tilde{x}_2$
1	$\tilde{x}_1 < \bar{x}_1$	$\tilde{x}_2 < \bar{x}_2$
2	$\bar{x}_1 < \tilde{x}_1$	$\bar{x}_2 < \tilde{x}_2$
3	$\bar{x}_1 < \tilde{x}_1$	$\tilde{x}_2 < \bar{x}_2$
4	$\tilde{x}_1 < \bar{x}_1$	$\bar{x}_2 < \tilde{x}_2$

In the next proposition, we will determine the multiplicity of the positive steady states of (1.2) according to the four cases in Table 1 as shown in Figures 2 and 3.

Proposition 2.8. *Assume that Hypotheses 2.1 and 2.2 hold. Let $S_{in} > \lambda_i(D)$, $i = 1, 2$.*

1. *In case 1 and 2, there exists at least one positive steady state. Generically, system (1.2) has an odd number of positive steady states.*
2. *In case 3 and 4, system (1.2) has generically no positive steady state or an even number of positive steady states.*

Note that the multiplicity of steady states of our model (1.2) and the four cases to be distinguished in Table 1, and Figures 2 and 3 are qualitatively similar to those of our density-dependence model in Fekih-Salem et al. [16].

3. Stability of steady states. To investigate the local asymptotic stability of all steady states of model (1.2), we shall use the abbreviation LES for Locally Exponentially Stable. Using notation (2.8), (2.11), and (2.13), the Jacobian matrix of model (1.2) at a steady state (S, x_1, x_2) is given by the following 3×3 matrix:

$$J = \begin{bmatrix} -D - E_1 x_1 - E_2 x_2 & -\mu_1(S) & -\mu_2(S) \\ E_1 x_1 & f_1 - Q_{11} x_1 & -Q_{12} x_1 \\ E_2 x_2 & -Q_{21} x_2 & f_2 - Q_{22} x_2 \end{bmatrix}.$$

The stability of the boundary steady states is given by the following result.

Proposition 3.1. *Under Hypotheses 2.1 and 2.2, we have*

- *$\mathcal{E}_0$ is LES if and only if $S_{in} < \min(\lambda_1, \lambda_2)$.*
- *$\mathcal{E}_1$ is LES if and only if $\bar{x}_1 < \tilde{x}_1$.*
- *$\mathcal{E}_2$ is LES if and only if $\bar{x}_2 < \tilde{x}_2$.*

Proof. For $\mathcal{E}_0 = (S_{in}, 0, 0)$, the characteristic polynomial is

$$P_0(\lambda) = (\lambda + D)(\lambda - (\mu_1(S_{in}) - D_1))(\lambda - (\mu_2(S_{in}) - D_2)).$$

Thus, $\mathcal{E}_0$ is LES if and only if $\mu_1(S_{in}) < D_1$ and $\mu_2(S_{in}) < D_2$, that is, $S_{in} < \lambda_1$ and $S_{in} < \lambda_2$.

For $\mathcal{E}_1 = (\tilde{S}_1, \tilde{x}_1, 0)$, the characteristic polynomial is

$$P_1(\lambda) = (\lambda - \lambda_0)\left(\lambda^2 + c_1\lambda + c_2\right),$$

where

$$\begin{aligned} \lambda_0 &= f_2(0, \tilde{x}_1) = \mu_2(S_{in} - g(\tilde{x}_1, 0)) - q_2(0, \tilde{x}_1) - D_2 \\ c_1 &= D + E_1\tilde{x}_1 + Q_{11}\tilde{x}_1 \\ c_2 &= (D + E_1\tilde{x}_1)Q_{11}\tilde{x}_1 + E_1\tilde{x}_1\mu_1(\tilde{S}_1). \end{aligned}$$

Since c_1 and c_2 are positive, then the roots of the quadratic factor have negative real parts. In addition, the function $x_1 \mapsto \mu_2(S_{in} - g(x_1, 0)) - q_2(0, x_1) - D_2$ is decreasing so that λ_0 is negative if and only if

$$\lambda_0 = \mu_2(S_{in} - g(\tilde{x}_1, 0)) - q_2(0, \tilde{x}_1) - D_2 < 0 = f_2(0, \bar{x}_1) = \mu_2(S_{in} - g(\bar{x}_1, 0)) - q_2(0, \bar{x}_1) - D_2.$$

Consequently, $\mathcal{E}_1$ is LES if and only if $\tilde{x}_1 > \bar{x}_1$.

For $\mathcal{E}_2 = (\tilde{S}_2, 0, \tilde{x}_2)$, the characteristic polynomial is

$$P_2(\lambda) = (\lambda - \lambda_0)\left(\lambda^2 + c_1\lambda + c_2\right),$$

where

$$\begin{aligned}
\lambda_0 &= f_1(0, \tilde{x}_2) = \mu_1(S_{in} - g(0, \tilde{x}_2)) - q_1(0, \tilde{x}_2) - D_1 \\
c_1 &= D + E_2\tilde{x}_2 + Q_{22}\tilde{x}_2 \\
c_2 &= (D + E_2\tilde{x}_2)Q_{22}\tilde{x}_2 + E_2\tilde{x}_2\mu_2(\tilde{S}_2).
\end{aligned}$$

Since c_1 and c_2 are positive, then the roots of the quadratic factor have negative real parts. In addition, the function $x_2 \mapsto \mu_1(S_{in} - g(0, x_2)) - q_1(0, x_2) - D_1$ is decreasing so that λ_0 is negative if and only if

$$\lambda_0 = \mu_1(S_{in} - g(0, \tilde{x}_2)) - q_1(0, \tilde{x}_2) - D_1 < 0 = f_1(0, \bar{x}_2) = 0 = \mu_1(S_{in} - g(0, \bar{x}_2)) - q_1(0, \bar{x}_2) - D_1.$$

Consequently, $\mathcal{E}_2$ is LES if and only if $\tilde{x}_2 > \bar{x}_2$. ∎

In the following, we study the stability of the positive steady states. Let J^* be the Jacobian matrix of (1.2) at a steady state $\mathcal{E}^* = (S^*, x_1^*, x_2^*)$, that is given by

$$J^* = \begin{bmatrix} -m_{11} & -m_{12} & -m_{13} \\ m_{21} & -m_{22} & -m_{23} \\ m_{31} & -m_{32} & -m_{33} \end{bmatrix},$$

where

$$\left\{ \begin{array}{lll}
m_{11} = D + E_1x_1^* + E_2x_2^*, & m_{12} = \mu_1(S^*), & m_{13} = \mu_2(S^*), \\
m_{21} = E_1x_1^*, & m_{22} = Q_{11}x_1^*, & m_{23} = Q_{12}x_1^*, \\
m_{31} = E_2x_2^*, & m_{32} = Q_{21}x_2^*, & m_{33} = Q_{22}x_2^*.
\end{array} \right. \tag{3.1}$$

Note that all m_{ij} are positive for all $i, j = 1, 2, 3$ and the functions Q_{ij} and E_i, $i, j = 1, 2$ defined by (2.11) and (2.13) are evaluated at the components of the positive steady state. Thus, the characteristic polynomial of J^* is given by

$$P(\lambda) = \lambda^3 + c_1\lambda^2 + c_2\lambda + c_3,$$

where

$$\begin{aligned}
c_1 &= m_{11} + m_{22} + m_{33}, \\
c_2 &= m_{11}(m_{22} + m_{33}) + m_{22}m_{33} + m_{12}m_{21} + m_{13}m_{31} - m_{23}m_{32}, \\
c_3 &= m_{11}(m_{22}m_{33} - m_{23}m_{32}) + m_{12}(m_{21}m_{33} - m_{23}m_{31}) + m_{13}(m_{22}m_{31} - m_{21}m_{32}).
\end{aligned} \tag{3.2}$$

As $c_1 > 0$, according to the Routh–Hurwitz criterion, the positive steady state $\mathcal{E}^*$ is LES if and only if

$$c_3 > 0 \quad \text{and} \quad c_4 = c_1c_2 - c_3 > 0. \tag{3.3}$$

The following result shows that the sign of c_3 is provided by the position of the curves γ_1 and γ_2 of functions $x_1 \mapsto F_1(x_1) = x_2$ and $x_1 \mapsto F_2^{-1}(x_1) = x_2$, respectively. More precisely, we will determine the relation between the determinant of the Jacobian matrix J^* at the positive steady state $\mathcal{E}^*$ and the value of $F_1'(x_1^*)F_2'(x_2^*) - 1$. Indeed, we will show that c_3 is negative [resp. positive] if and only if $F_1'(x_1^*)\,F_2'(x_2^*) - 1$ is negative [resp. positive], that is,

$$F_1'(x_1^*) > \left(F_2^{-1}\right)'(x_1^*) = \frac{1}{F_2'(x_2^*)} \quad \left[\text{resp. } F_1'(x_1^*) < \left(F_2^{-1}\right)'(x_1^*)\right]$$

because $F_2'(x_2^*) < 0$, or equivalently, on the right of the positive steady state (x_1^*, x_2^*), the tangent of γ_1 at this point (x_1^*, x_2^*) is above [resp. under] the tangent of γ_2 at the same point (x_1^*, x_2^*) (see Figures 2 and 3).

Proposition 3.2. *Let $\mathcal{E}^* = (S^*, x_1^*, x_2^*)$ be a positive steady state of (1.2). We have*

$$c_3 = -\det(J^*) = Dx_1^*x_2^*(F_1'(x_1^*)F_2'(x_2^*) - 1)(E_1G_2 + Q_{12})(E_2G_1 + Q_{21}), \tag{3.4}$$

where the functions E_i, G_i and Q_{ij} are defined by (2.10), (2.11), and (2.13) and are evaluated at the components of the steady state $\mathcal{E}^*$.

Proof. Using the expression of the derivatives of F_i given by (2.12), a straightforward calculation shows that

$$F_1'(x_1^*)F_2'(x_2^*) - 1 = \frac{(Q_{11}Q_{22} - Q_{12}Q_{21}) + G_1(E_1Q_{22} - E_2Q_{12}) + G_2(E_2Q_{11} - E_1Q_{21})}{(E_1G_2 + Q_{12})(E_2G_1 + Q_{21})}. \tag{3.5}$$

Let L_i, $i = 1, 2, 3$ be the lines of the matrix J^*. The replacement of L_1 by $L_1 + L_2 + L_3$ preserves the determinant of the Jacobian matrix J^* at the steady state $\mathcal{E}^*$ and we obtain

$$c_3 = -\begin{vmatrix} -D & -\mu_1(S^*) - Q_{11}x_1^* - Q_{21}x_2^* & -\mu_2(S^*) - Q_{12}x_1^* - Q_{22}x_2^* \\ E_1x_1^* & -Q_{11}x_1^* & -Q_{12}x_1^* \\ E_2x_2^* & -Q_{21}x_2^* & -Q_{22}x_2^* \end{vmatrix}.$$

By expanding along the first line, we obtain

$$\begin{aligned} c_3 = x_1^*x_2^*[&D(Q_{11}Q_{22} - Q_{12}Q_{21}) + (\mu_1(S^*) + Q_{11}x_1^* + Q_{21}x_2^*)(E_1Q_{22} - E_2Q_{12}) + \\ &(\mu_2(S^*) + Q_{12}x_1^* + Q_{22}x_2^*)(E_2Q_{11} - E_1Q_{21})]. \end{aligned}$$

Recall that, at the positive steady state $\mathcal{E}^*$, we have

$$\mu_1(S^*) = q_1(x_1^*, x_2^*) + D_1 \quad \text{and} \quad \mu_2(S^*) = q_2(x_2^*, x_1^*) + D_2.$$

Using (2.10), it follows that

$$\begin{cases} \mu_1(S^*) + Q_{11}x_1^* + Q_{21}x_2^* = q_1(x_1^*, x_2^*) + D_1 + Q_{11}x_1^* + Q_{21}x_2^* = DG_1, \\ \mu_2(S^*) + Q_{22}x_2^* + Q_{12}x_1^* = q_2(x_2^*, x_1^*) + D_2 + Q_{22}x_2^* + Q_{12}x_1^* = DG_2. \end{cases}$$

Consequently,

$$c_3 = Dx_1^*x_2^*\left[(Q_{11}Q_{22} - Q_{12}Q_{21}) + G_1(E_1Q_{22} - E_2Q_{12}) + G_2(E_2Q_{11} - E_1Q_{21})\right].$$

The expression of c_3 given by (3.4) follows by using relation (3.5). ∎

Thus, we determine in the following proposition the sufficient conditions of instability and stability of a positive steady state of model (1.2).

Proposition 3.3. *Let $\mathcal{E}^* = (S^*, x_1^*, x_2^*)$ be a positive steady state of model (1.2).*
1. *When $F_1'(x_1^*)\,F_2'(x_2^*) < 1$, $\mathcal{E}^*$ is unstable.*
2. *When $Q_{11}Q_{22} \geq Q_{12}Q_{21}$ holds, $\mathcal{E}^*$ is LES if and only if $F_1'(x_1^*)\,F_2'(x_2^*) > 1$.*

Proof. Since all the functions E_i, G_i and Q_{ij} in (3.4) evaluated at $\mathcal{E}^*$ are positive, then from Proposition 3.2, we have $c_3 < 0$ when $F_1'(x_1^*)\,F_2'(x_2^*) < 1$. The first assertion of the proposition follows from the first condition of the Routh–Hurwitz criterion in (3.3).

Using the coefficients c_i of the characteristic polynomial of J^* given by (3.2), straightforward calculations show that

$$\begin{aligned} c_4 = \; & D(c_2 + Q_{12}Q_{21}x_1^*x_2^*) + (E_1x_1^* + E_2x_2^*)(m_{11}(m_{22}+m_{33}) + m_{12}m_{21} + m_{13}m_{31}) \\ & + D((Q_{11}x_1^*)^2 + (Q_{22}x_2^*)^2 + Q_{11}Q_{22}x_1^*x_2^*) + (E_1x_1^* + E_2x_2^*)(Q_{11}x_1^* + Q_{22}x_2^*)^2 \\ & + (Q_{11}x_1^* + Q_{22}x_2^*)(Q_{11}Q_{22} - Q_{12}Q_{21})x_1^*x_2^* + \mu_1(S^*)E_1Q_{11}(x_1^*)^2 \\ & + \mu_2(S^*)E_2Q_{22}(x_2^*)^2 + \mu_1(S^*)E_2Q_{12}x_1^*x_2^* + \mu_2(S^*)E_1Q_{21}x_1^*x_2^*, \end{aligned} \tag{3.6}$$

where Q_{ij}, E_i, m_{ij}, and c_2 are defined in (2.11), (2.13), (3.1), and (3.2). Note that all terms in the expression of c_4 in (3.6) are positive, except $Q_{11}Q_{22} - Q_{12}Q_{21}$ which can be negative. If $Q_{11}Q_{22} \geq Q_{12}Q_{21}$, that is, $m_{22}m_{33} - m_{23}m_{32} \geq 0$, it follows from (3.2) that $c_2 > 0$. Moreover, from (3.6), we obtain $c_4 > 0$ in this case. Consequently, $\mathcal{E}^*$ is LES if and only if $c_3 > 0$, that is, $F_1'(x_1^*)\,F_2'(x_2^*) > 1$. ∎

When $Q_{11}Q_{22} \geq Q_{12}Q_{21}$, the local stability of positive steady states is completely characterized by the position of the curves γ_1 and γ_2. When this condition does not hold, we were not able to prove that c_4 is always positive or to find a set of parameters such that c_4 changes sign and becomes negative. This question remains an open problem and deserves further investigations.

Here, the condition $Q_{11}Q_{22} \geq Q_{12}Q_{21}$ are qualitatively similar to condition (26) in [16] which means that the intraspecific interference is dominant with respect to interspecific interference. However, in our particular model (1.1), this condition becomes

$$(a_{11} + \alpha_1x_2^2)(a_{22} + \alpha_2x_1^2) > (a_{12} + 2\alpha_1x_1x_2)(a_{21} + 2\alpha_2x_1x_2).$$

where it does not only depend on intra- and interspecific interference as in [16] but it also depends on the quadratic forms representing allelopathic effects of the two species. Moreover, contrary to our density-dependence model [16], the condition $c_4 > 0$ of the Routh–Hurwitz criterion (3.3) should be verified in the case of the same removal rate ($D_1 = D_2 = D$). Thus, the addition of mortality is necessary for the model [16] to hope for destabilization of the coexistence steady state but in our model (1.2) mortality is not necessary.

4. Operating diagram.

The operating diagram is a very useful visual representation for mathematicians and biologists because it provides a summary and an overall view of the behavior of the process according to the control parameters [27, 50]. In the existing literature, the study of the operating diagram is classified into three different methods. In the following, we synthesize the main characteristics of each method, specifying the advantages and disadvantages. However, for more on these various methods, the reader is referred to [41] and the references therein.

The first method consists in determining the various regions of the operating diagram by numerically solving the algebraic equations giving the steady states having all the nonnegative components. Then, the sign of the roots of the characteristic polynomial determines the local asymptotic behavior of each steady state [53]. This method can be used for complex dynamic systems including a very large number of variables and parameters [25, 31, 55, 57]. However, this method is time-consuming in computation. In addition, some regions of sufficiently small sizes than the step used for the discretization of the operating parameters could be omitted. Sari et al. [42, 43, 44, 48] demonstrated that regions of coexistence around a stable limit cycle were not detected in the study of the numerical operating diagram of a process describing the anaerobic mineralization of chlorophenol in a three-step food-web [54].

The second method is numerical and consists in determining the boundaries of the various regions of the operating diagram using a numerical continuation and correction algorithm. Various software packages have been developed to solve continuation and bifurcation problems in systems of autonomous ODEs depending on one or two parameters. The most used are MATCONT, CONTENT, AUTO, and XPPAUT (see [13] and the reference therein). This method has the advantage of detecting more complex and subtle bifurcations such as the bifurcations of types limit point of cycles, cusp, Bogdanov-Takens, Bautin, etc (see for example [51]).

The third method is theoretical and consists in determining the borders of the various regions from the analytical study of the model by establishing the conditions of existence and stability of all steady states according to the operating parameters. The disadvantage of this method is the difficulty of analyzing complex models and illustrating the various curves in some cases with several state variables. However, this method allows us to detect all the regions of the operating diagram [1, 3, 8, 10, 11, 12, 13, 16, 14, 40, 41, 44, 46, 47, 48].

We shall now study theoretically and numerically the operating diagram of system (1.2). It is the most useful tool for biologists describing qualitatively the asymptotic behavior of the process according to the operating parameters of the model. Here, the operating parameters are the concentration of substrate in the feed bottle S_{in} and the dilution rate D.

Table 2

Necessary and sufficient conditions of existence and local stability of all steady states of (1.2) where c_4 is defined by (3.6).

	Existence	Local stability
$\mathcal{E}_0$	always exists	$S_{in} < \min(\lambda_1(D), \lambda_2(D))$
$\mathcal{E}_1$	$S_{in} > \lambda_1(D)$	$\bar{x}_1(S_{in}, D) < \tilde{x}_1(S_{in}, D)$
$\mathcal{E}_2$	$S_{in} > \lambda_2(D)$	$\bar{x}_2(S_{in}, D) < \tilde{x}_2(S_{in}, D)$
$\mathcal{E}^*$	Equation (2.14) has a solution	$F_1'(x_1^*)\,F_2'(x_2^*) > 1$ and $c_4(S_{in}, D) > 0$

To study the operating diagram in the next section, the necessary and sufficient conditions for the existence and local stability of all steady states of (1.2) are summarized in Table 2. From these conditions, we define in Table 3, the set $\Upsilon = \{\Upsilon_1, \Upsilon_2, \Upsilon_3, \Upsilon_4, \Upsilon_5\}$ of all boundaries between various regions of the (S_{in}, D)-plane. More precisely, when the curves γ_1 and γ_2 of the functions $x_1 \mapsto F_1(x_1)$ and $x_2 \mapsto F_2(x_2)$ are tangent in a point (x_1, x_2), we have

$$x_2 = F_1(x_1), \quad x_1 = F_2(x_2), \quad \text{and} \quad F_1'(x_1)F_2'(x_2) = 1. \tag{4.1}$$

The solution (x_1, x_2) of this set of equations depends on S_{in} and D. Hence, we can define in Table 3 the subset Υ_5 which represents a curve in the generic case (see Figure 5). As we will see in section 5, passing through Υ_5 in the operating plan (S_{in}, D) gives rise to two positive steady states via a saddle-node bifurcation. Moreover, the passages through the subsets Υ_1 and Υ_2 generate the steady states $\mathcal{E}_1$ and $\mathcal{E}_2$, respectively, that coalesce with the washout steady state $\mathcal{E}_0$ via a transcritical bifurcation. Finally, crossing the curves Υ_3 and Υ_4, a positive steady state appears or disappears through the coalescence with the steady states $\mathcal{E}_1$ and $\mathcal{E}_2$, respectively, corresponding to a transcritical bifurcation.

Table 3

The set Υ and the corresponding colors in Figure 4 and Figure 5.

Υ	Color
$\Upsilon_1 = \{(S_{in}, D) : S_{in} = \lambda_1(D)\}$	Blue
$\Upsilon_2 = \{(S_{in}, D) : S_{in} = \lambda_2(D)\}$	Red
$\Upsilon_3 = \{(S_{in}, D) : \tilde{x}_1(S_{in}, D) = \bar{x}_1(S_{in}, D)\}$	Cyan
$\Upsilon_4 = \{(S_{in}, D) : \tilde{x}_2(S_{in}, D) = \bar{x}_2(S_{in}, D)\}$	Magenta
$\Upsilon_5 = \{(S_{in}, D) : x_2 = F_1(x_1),\ x_1 = F_2(x_2),\ \text{and } F_1'(x_1)F_2'(x_2) = 1\}$	Green

Now, to illustrate the operating diagram, we consider model (1.2) and we choose the following specific growth rates of Monod-type satisfying Hypotheses 2.1 and 2.2:

$$\mu_1(S) = \frac{\mu_1^m S}{k_1 + S}, \quad \mu_2(S) = \frac{\mu_2^m S}{k_2 + S}, \tag{4.2}$$

where μ_1^m and μ_2^m are the maximum growth rates; k_1 and k_2 are the Michaelis-Menten constants. The values of these biological parameters are provided in Table 14. As in particular model (1.1), the functions q_1 and q_2 representing the intra- and interspecific interactions with the allelopathic competitions of the two species take the form

$$q_1(x_1, x_2) = a_{11}x_1 + a_{12}x_2 + \alpha_1 x_1 x_2^2, \quad q_2(x_2, x_1) = a_{22}x_2 + a_{21}x_1 + \alpha_2 x_2 x_1^2. \tag{4.3}$$

The construction of this diagram is similar for any other specific growth rate satisfying Hypotheses 2.1 and 2.2. Except for the control parameters S_{in} and D, all the biological parameters are fixed since they depend on the nature of the organisms, the substrate introduced into the bioreactor, and the various interactions between the species. All the values of these parameters used throughout this paper are provided in Table 14.

For this set of parameter values, Appendix A shows that the stability condition $c_4 > 0$ holds for all S_{in} and D in the existence domain of $\mathcal{E}_1^*$ and $\mathcal{E}_3^*$. Thus, there can be no destabilization of a coexistence steady state via a Hopf bifurcation with the emergence of a cycle limit. Note that the steady state $\mathcal{E}_2^*$ is unstable when it exists because c_3 is negative. Consequently, the only curves separating the various regions in the operating diagram are given by Υ_i, $i = 1, \ldots, 5$. MAPLE [36] was able to plot the curves Υ_i, $i = 1, \ldots, 4$ (see Figure 4) except the curve Υ_5 where it must resolve the three equations in (4.1) with two variables and two unknown parameters.

The concept of *steady state characteristic* that was introduced by Lobry et al. [34, 35] could reduce the number of variables by expressing the concentrations of the biomass x_1

and x_2 as a function of the concentration of the substrate S (see [18] for more details). Hence, to determine all the components of the positive steady state, it suffices to determine the variable S which can be deduced from the resolution of an equation of the system at a positive steady state where S is the single variable. In some cases, this reduction would allow to determine in MAPLE all the curves of the operating diagram (see for example [41]). However, this method of *steady state characteristic* cannot be applied to our general model (1.2) to plot in MAPLE the saddle-node bifurcation curve Υ_5 because of the structure of model where the equations at a positive steady state depend on three variables. In section 6, we will show that this method can be used in particular model (1.2) of Kengwoung-Keumo [30] where $q_2(x_2, x_1) = a_{11} = a_{12} = 0$, that is, without intra- and interspecific interference in the dynamics of the two species and without the allelopathic competition of the first species on the second species.

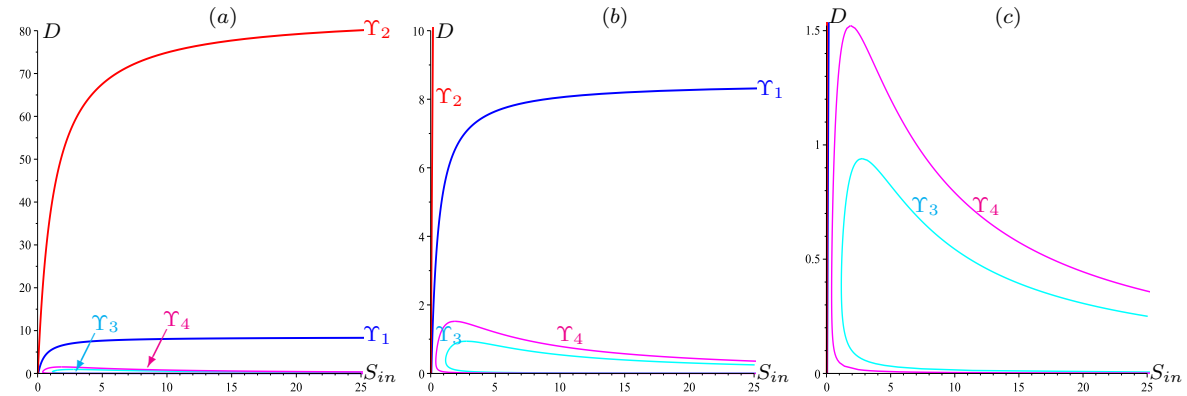

Figure 4. *MAPLE: (a) curves* Υ_i, $i = 1, \ldots, 4$. *(b)-(c) Magnification when* $(S_{in}, D) \in [0, 25] \times [0, 10]$ *and* $(S_{in}, D) \in [0, 25] \times [0, 1.5]$, *respectively.*

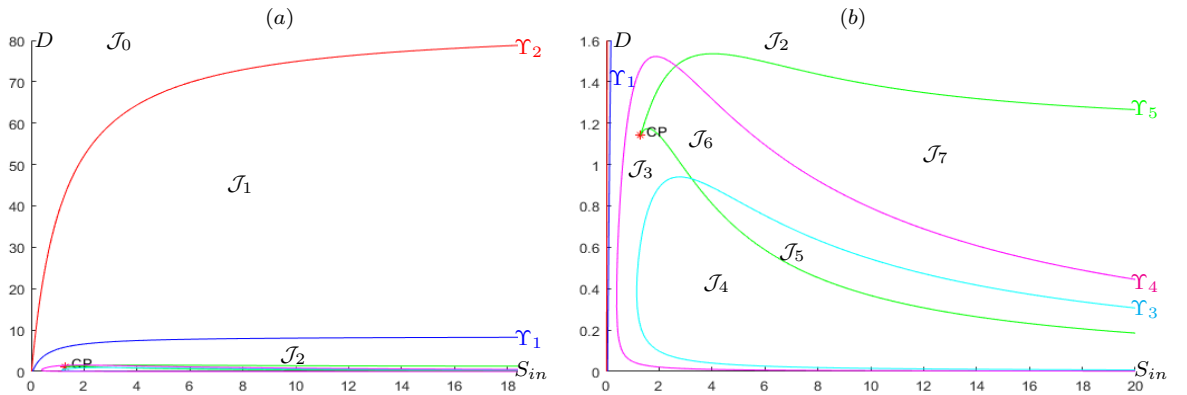

Figure 5. *MATCONT: (a) operating diagram of* (1.2). *(b) Magnification when* $(S_{in}, D) \in [0, 20] \times [0, 1.6]$.

Figure 4 illustrates the theoretical operating diagram obtained in MAPLE by drawing the curves Υ_i, $i = 1, \ldots, 4$ defined in Table 3 but the curve Υ_5 is missing which corresponds to the saddle-node bifurcation.

To solve the numerical problem in MAPLE determining the saddle-node bifurcation curve

Υ_5, we use in the following the numerical method to determine the operating diagram of model (1.2) with the software MATCONT [38]. Indeed, MATCONT is a MATLAB numerical continuation package for the interactive bifurcation study of continuous and discrete parameterized systems of ODEs. It allows one to compute curves of steady states and limit cycles (periodic orbits), and their bifurcations as Branch Points (BP) or transcritical bifurcations, Limit Points (LP) or saddle-node (or fold) bifurcations, Cusp bifurcations (CP), Hopf points (H), Limit Point of Cycles (LPC) or fold bifurcation points of limit cycles, and period doubling bifurcation points of limit cycles. For more on this interesting subject, the reader is referred to [13] and the references therein.

Figure 5 illustrates the numerical operation diagram obtained using MATCONT by drawing the curves Υ_i, $i = 1, \ldots, 5$. For $i = 1, \ldots, 4$, the curves Υ_i are identical in the theoretical and the numerical operating diagrams. Thus, we obtain the following result giving a complete description of the operating diagram.

Proposition 4.1. *For the specific growth rates μ_1 and μ_2 defined in (4.2), the functions q_1 and q_2 defined in (4.3), and the set of the biological parameter values in Table 14, the existence and the local stability of all steady states of (1.2) in the eight regions $\mathcal{J}_k$, $k = 0, \ldots, 7$ of the operating diagram in Figure 5 are described in Table 4.*

Table 4

Existence and local stability of all steady states in the various regions of the operating diagram in Figure 5. The letter S [resp. U] means stable [resp. unstable] steady state. Absence of letter means that the corresponding steady state does not exist.

Region	$\mathcal{E}_0$	$\mathcal{E}_1$	$\mathcal{E}_2$	$\mathcal{E}_1^*$	$\mathcal{E}_2^*$	$\mathcal{E}_3^*$
$\mathcal{J}_0$	S					
$\mathcal{J}_1$	U		S			
$\mathcal{J}_2$	U	U	S			
$\mathcal{J}_3$	U	U	U	S		
$\mathcal{J}_4$	U	S	U			
$\mathcal{J}_5$	U	S	U	S	U	
$\mathcal{J}_6$	U	U	U	S	U	S
$\mathcal{J}_7$	U	U	S	S	U	

The operating diagram in Figure 5 is divided into eight regions. The region $\mathcal{J}_0$ corresponds to the washout of two species. The regions $\mathcal{J}_1$ and $\mathcal{J}_2$ [resp. $\mathcal{J}_4$] correspond to the competitive exclusion of the first [resp. second] species. The region $\mathcal{J}_3$ corresponds to the coexistence of both species. The region $\mathcal{J}_5$ [resp. $\mathcal{J}_7$] corresponds to the bistability with either coexistence or exclusion of the second [resp. first] species. The region $\mathcal{J}_6$ corresponds to the bistability with convergence to one of the two coexistence steady states.

5. Analysis of bifurcations. In this section, we will first study the different types of bifurcation by passing from one region to another in the two-parameter operating diagram. Next, we will analyze the one-parameter bifurcation diagram. The following result describes the nature of all the bifurcations that occur by crossing one region to another through the various curves in the set Υ defined in Table 3.

Proposition 5.1. *The nature of all the bifurcations of the steady states of system (1.2) by passing between the various regions of the operating diagram is provided in Table 5.*

Table 5

Nature of all the bifurcations of the steady states of model (1.2) by crossing the various curves in the set Υ. The letter BP (resp. LP) means a Branch Point (resp. Limit Point) bifurcation.

Transition	Curve	Bifurcation	Steady states
$\mathcal{J}_0$ to $\mathcal{J}_1$	Υ_2	BP	$\mathcal{E}_0 = \mathcal{E}_2$
$\mathcal{J}_1$ to $\mathcal{J}_2$	Υ_1	BP	$\mathcal{E}_0 = \mathcal{E}_1$
$\mathcal{J}_2$ to $\mathcal{J}_3$	Υ_4	BP	$\mathcal{E}_2 = \mathcal{E}_1^*$
$\mathcal{J}_2$ to $\mathcal{J}_7$	Υ_5	LP	$\mathcal{E}_1^* = \mathcal{E}_2^*$
$\mathcal{J}_3$ to $\mathcal{J}_6$	Υ_5	LP	$\mathcal{E}_2^* = \mathcal{E}_3^*$
$\mathcal{J}_3$ to $\mathcal{J}_4$	Υ_3	BP	$\mathcal{E}_1 = \mathcal{E}_1^*$
$\mathcal{J}_4$ to $\mathcal{J}_5$	Υ_5	LP	$\mathcal{E}_1^* = \mathcal{E}_2^*$
$\mathcal{J}_5$ to $\mathcal{J}_6$	Υ_3	BP	$\mathcal{E}_1 = \mathcal{E}_3^*$
$\mathcal{J}_6$ to $\mathcal{J}_7$	Υ_4	BP	$\mathcal{E}_2 = \mathcal{E}_3^*$

Now to illustrate the nature of bifurcations by passing through the boundaries of the different regions of the operating diagram studied in section 4, we study the one-parameter bifurcation diagram. The dilution rate D is considered as a bifurcation parameter. However, the one-parameter bifurcation diagram in S_{in} can be obtained in the same way. Throughout this section, we assume that the parameters μ_i^m, k_i, a_{ii}, a_{ij}, α_i, θ_i and m_i, $i = 1, 2$, $j = 1, 2$, $i \neq j$ are fixed at the values provided in Table 14. To maximize the passage number through the various regions of the operating diagram in Figure 5, the inflowing concentration was fixed at $S_{in} = 1.4$. Using MATCONT [38], we plot in Figure 6 the one-parameter bifurcation diagram in D, with S, x_1 and x_2 on the y-axis. This diagram corresponds to a vertical line of equation $S_{in} = 1.4$ in the operating diagram of Figure 5.

First, by increasing D from zero, the one-parameter bifurcation diagram in the variable S in Figure 6(a) illustrates the Branch Point (BP) bifurcation or the transcritical bifurcation occurring at $D = \sigma_1 \approx 0.032$ between $\mathcal{E}_2$ and $\mathcal{E}_1^*$. In fact, the steady state of exclusion of the first species $\mathcal{E}_2$ becomes unstable while the coexistence steady state $\mathcal{E}_1^*$ emerges LES into the interior of the admissible region. Since the first bifurcations occur for small values of D, a first close-up is presented in Figure 6(b) and a second close-up is presented in Figure 6(c). The one-parameter bifurcation diagrams in D presented in Figure 6(d-g) with x_1 and x_2 on the y-axis show the same bifurcation values σ_i, $i = 1, \ldots, 8$ defined in Table 7 and determine the different components of steady states and their local stability.

Next, there is a BP bifurcation at $D = \sigma_2 \approx 0.181$ between $\mathcal{E}_1^*$ and $\mathcal{E}_1$ such that the interior steady state $\mathcal{E}_1^*$ disappears while $\mathcal{E}_1$ becomes LES. After that, once again a BP bifurcation occurs at $D = \sigma_3 \approx 0.692$ between $\mathcal{E}_1$ and $\mathcal{E}_1^*$ where this last coexistence steady state appears LES while $\mathcal{E}_1$ becomes unstable. Increasing D further, a Limit Points (LP) or saddle-node bifurcation occurs that gives birth to unstable and stable positive steady states $\mathcal{E}_2^*$ and $\mathcal{E}_3^*$, respectively, at $D = \sigma_4 \approx 1.163$. Next, the stable and unstable steady states $\mathcal{E}_1^*$ and $\mathcal{E}_2^*$ collide at $D = \sigma_5 \approx 1.182$ and disappear through an LP bifurcation. After that, there is a BP bifurcation at $D = \sigma_6 \approx 1.485$ between $\mathcal{E}_3^*$ and $\mathcal{E}_2$ where the steady state $\mathcal{E}_3^*$ disappears

while $\mathcal{E}_2$ becomes LES. Increasing D further, a BP bifurcation occurs at $D = \sigma_7 \approx 6.033$ between $\mathcal{E}_0$ and $\mathcal{E}_1$ where the steady state $\mathcal{E}_1$ disappears while $\mathcal{E}_0$ remains unstable. Finally, a BP bifurcation occurs at $D = \sigma_8 \approx 44.769$ between $\mathcal{E}_0$ and $\mathcal{E}_2$ such that $\mathcal{E}_0$ becomes LES while $\mathcal{E}_2$ disappears from the nonnegative quadrant.

The following result summarizes the study of this one-parameter bifurcation diagram in D from the operating diagram in Figure 5.

Proposition 5.2. *For the specific growth rates μ_1 and μ_2 (4.2), the functions q_1 and q_2 defined in (4.3), and the set of the biological parameter values in Table 14, the existence and the local stability of all steady states of (1.2) according to D are described in Table 6 when $S_{in} = 1.4$ is fixed. The critical values σ_i, $i = 1, \ldots, 8$ of different bifurcations according to the parameter D and the corresponding nature are defined in Table 7.*

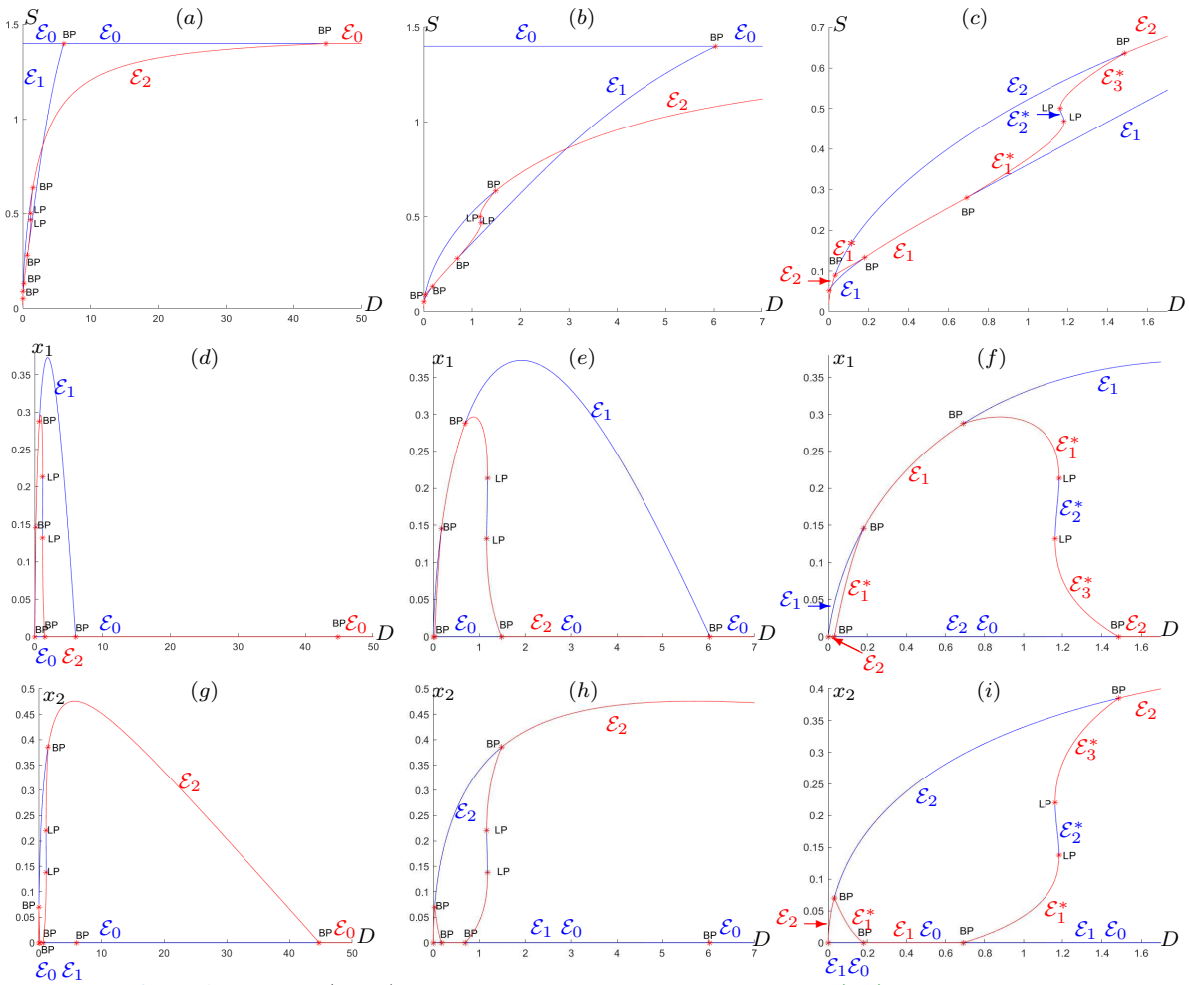

Figure 6. *MATCONT: (a-d-g) one-parameter bifurcation diagrams of (1.2) in the variables S, x_1, x_2, (resp.), with D as the bifurcation parameter and $S_{in} = 1.4$; (b-e-h) (resp. (c-f-i)) magnifications when $D \in [0, 7]$ (resp. $D \in [0, 1.7]$); Red (resp. Blue) curve represents the continuation of a stable (resp. unstable) steady state.*

Table 6

Existence and stability of steady states according to D where σ_i, $i = 1, \ldots, 8$ are defined in Table 7.

Interval of D	$\mathcal{E}_0$	$\mathcal{E}_1$	$\mathcal{E}_2$	$\mathcal{E}_1^*$	$\mathcal{E}_2^*$	$\mathcal{E}_3^*$
$(0, \sigma_1)$	U	U	S			
(σ_1, σ_2)	U	U	U	S		
(σ_2, σ_3)	U	S	U			
(σ_3, σ_4)	U	U	U	S		
(σ_4, σ_5)	U	U	U	S	U	S
(σ_5, σ_6)	U	U	U			S
(σ_6, σ_7)	U	U	S			
(σ_7, σ_8)	U		S			
$(\sigma_8, +\infty)$	S					

Table 7

Definitions of the critical values σ_i, $i = 1, \ldots, 8$ of D and the corresponding nature of bifurcations when $S_{in} = 1.4$ is fixed.

Definition	Value	Bifurcation
σ_1 is the first solution of equation $\tilde{x}_2(S_{in}, D) = \bar{x}_2(S_{in}, D)$	0.032	BP
σ_2 is the first solution of equation $\tilde{x}_1(S_{in}, D) = \bar{x}_1(S_{in}, D)$	0.181	BP
σ_3 is the second solution of equation $\tilde{x}_1(S_{in}, D) = \bar{x}_1(S_{in}, D)$	0.692	BP
σ_4 is the first solution of equation $c_3(S_{in}) = 0$	1.163	LP
σ_5 is the second solution of equation $c_3(S_{in}) = 0$	1.182	LP
σ_6 is the second solution of equation $\tilde{x}_2(S_{in}, D) = \bar{x}_2(S_{in}, D)$	1.485	BP
$\sigma_7 = \mu_1(S_{in})$	6.033	BP
$\sigma_8 = \mu_2(S_{in})$	44.769	BP

6. Application to the particular model of Kengwoung-Keumo. Our general model (1.2) was studied by Kengwoung-Keumo [30] in the particular case where the functions $q_2(x_2, x_1) = 0$ and $q_1(x_1, x_2) = \alpha_1 x_1 x_2^2$ so that $a_{11} = a_{12} = a_{22} = a_{21} = 0$, that is, without the effect of intra- and interspecific interference of the two species and without the allelopathic effect of the first species on the second species. Recall that kengwong-Keumo's particular model is written as follows where the yield coefficients are normalized to the unit:

$$\left\{ \begin{array}{rcl} \dot{S} & = & D(S_{in} - S) - \mu_1(S)x_1 - \mu_2(S)x_2, \\ \dot{x}_1 & = & [\mu_1(S) - \alpha_1 x_1 x_2^2 - D_1]x_1, \\ \dot{x}_2 & = & [\mu_2(S) - D_2]x_2. \end{array} \right. \tag{6.1}$$

In what follows, we apply our theoretical results of existence and stability of all steady states of the general model (1.2) to those of the particular model (6.1) by comparing our results found with those in [30]. Next, we will also analyze the operating diagram and the one-parameter bifurcation diagram of model (6.1) which have not been studied in [30].

In order to analyze the existence of the positive steady states of system (6.1), we can use the method presented in section 2 by writing the variable x_j, $j = 1, 2$ as a function F_i, $i = 1, 2$, $i \neq j$ of the variable x_i from the equation $f_i(x_i, x_j) = 0$ defined in (2.8). However, in the following, we will use the concept of *steady state characteristic* due to the particularity of the

structure of system (6.1) to give explicit expressions of the components of the positive steady states by determining their multiplicities and their existence conditions. The advantage of this method is that it will allow us to theoretically determine all the curves of the operating diagram in the plane (S_{in}, D) without having recourse to MATCONT to draw the curve Υ_5 which corresponds to a saddle-node bifurcation. To do this, we begin by setting the right-hand sides of equations in (6.1) equal to zero:

$$D(S_{in} - S) - \mu_1(S)x_1 - \mu_2(S)x_2 = 0, \tag{6.2}$$

$$[\mu_1(S) - \alpha_1 x_1 x_2^2 - D_1]x_1 = 0, \tag{6.3}$$

$$[\mu_2(S) - D_2]x_2 = 0. \tag{6.4}$$

- For $\mathcal{E}_0$, $x_1 = x_2 = 0$. Hence, (6.2) results in $S = S_{in}$. Thus, $\mathcal{E}_0$ always exists.
- For $\mathcal{E}_1$, $x_2 = 0$ and $x_1 > 0$. Hence, (6.2) and (6.3) result in $S = \lambda_1$ and $x_1 = D(S_{in} - \lambda_1)/D_1$. Hence, $\mathcal{E}_1$ exists if and only if $S_{in} > \lambda_1$.
- For $\mathcal{E}_2$, $x_1 = 0$ and $x_2 > 0$. Hence, (6.2) and (6.4) result in $S = \lambda_2$ and $x_2 = D(S_{in} - \lambda_2)/D_2$. Hence, $\mathcal{E}_2$ exists if and only if $S_{in} > \lambda_2$.
- For $\mathcal{E}^*$, $x_1 > 0$ and $x_2 > 0$. Hence, (6.4) results in $S = \lambda_2$. Moreover, (6.3) results

$$x_1 = H(x_2) := \frac{a^+}{x_2^2}, \quad \text{with} \quad a^+ = \frac{\mu_1(\lambda_2) - D_1}{\alpha_1}. \tag{6.5}$$

Hence, a necessary condition for the positivity of the component x_1 is that a^+ be positive,

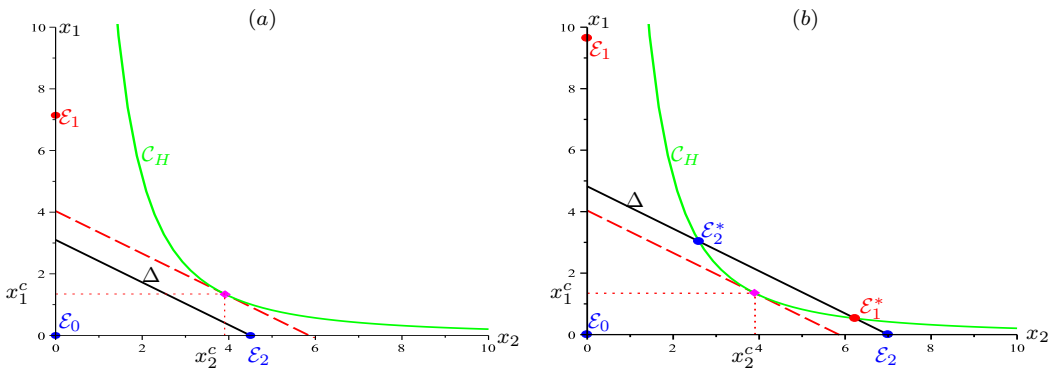

Figure 7. *Existence and stability of steady states of model (6.1) when $D = 5$: (a) $S_{in} = 8 < S_{in}^c \approx 9.357$, (b) $S_{in} = 10.5 > S_{in}^c$. In all figures, we use the red [resp. blue] color for LES [resp. unstable] steady state.*

that is, $\lambda_1 < \lambda_2$. In addition, (6.2) results in

$$x_1 = \delta(x_2) := b^+ - c^+ x_2, \quad \text{with} \quad b^+ = \frac{D(S_{in} - \lambda_2)}{\mu_1(\lambda_2)}, \quad c^+ = \frac{D_2}{\mu_1(\lambda_2)}. \tag{6.6}$$

Since c^+ is positive, a necessary condition for the positivity of the component x_1 is that b^+ be positive, that is, $\lambda_2 < S_{in}$. Thus, system (6.1) has a positive steady state $\mathcal{E}^* = (\lambda_2, x_1^*, x_2^*)$ if and only if the curve $\mathcal{C}_H$ of the function $x_2 \mapsto H(x_2)$ and the straight line Δ of equation

$x_1 = \delta(x_2)$ have a positive intersection (see Figure 7) such that the coordinates (x_1^*, x_2^*) are positive solutions of equations

$$x_1 = H(x_2) \quad \text{and} \quad x_1 = \delta(x_2),$$

or equivalently, these solutions satisfy the necessary condition $\lambda_1 < \lambda_2 < S_{in}$. Using expression (6.5) of the function H, we have

$$H'(x_2) = -2\frac{a^+}{x_2^3} < 0 \quad \text{and} \quad H''(x_2) = 6\frac{a^+}{x_2^4} > 0.$$

Thus, the function H is convex (see Figure 7) with $H(0^+) = +\infty$ and $H(+\infty) = 0$. Consequently, there are at most two solutions of equation $H(x_2) = \delta(x_2)$. Let ϕ be the function defined by

$$\phi(x_2) := H'(x_2) - \delta'(x_2) = H'(x_2) + c^+.$$

Since ϕ is increasing from $\phi(0^+) = -\infty$ to $\phi(+\infty) = c^+$, then for all $D > 0$ there exists a unique solution

$$x_2 = x_2^c(D) := \sqrt[3]{\frac{2a^+}{c^+}}$$

of equation $H'(x_2) = \delta'(x_2)$. If in addition, for all $D > 0$, $H(x_2^c) = \delta(x_2^c)$, then there exists a unique critical value of S_{in} denoted $S_{in}^c(D)$ that we determine in the following its explicit expression. Indeed, from (6.5) and (6.6), it follows that $H(x_2^c) = \delta(x_2^c)$ is equivalent to

$$\frac{a^+}{(x_2^c)^2} = b^+ - c^+ x_2^c.$$

Then, using the expressions of a^+, b^+ and c^+ in (6.5) and (6.6), straightforward calculation shows that

$$S_{in}^c(D) = \lambda_2 + \frac{3}{D}\sqrt[3]{\frac{D_2^2\mu_1(\lambda_2)(\mu_1(\lambda_2) - D_1)}{4\alpha_1}}. \tag{6.7}$$

Consequently, a positive steady state $\mathcal{E}^*$ exists if and only if $\lambda_1(D) < \lambda_2(D)$ and $S_{in} > S_{in}^c$. Next, the local stability of all steady states of system (6.1) is deduced from that in section 3 by taking $q_2(x_2, x_1) = 0$ and $q_1(x_1, x_2) = \alpha_1 x_1 x_2^2$. From Proposition 3.1, $\mathcal{E}_0$ is LES if and only if $S_{in} < \min(\lambda_1, \lambda_2)$. Moreover, $\mathcal{E}_1$ is LES if and only if $\bar{x}_1 < \tilde{x}_1$ which is equivalent to $\lambda_1(D) < \lambda_2(D)$. Indeed, from Proposition 2.4, $\tilde{x}_1$ is the unique solution of equation

$$\psi_1(x_1) = \mu_1(\varphi_1(x_1)) - D_1 - q_1(x_1, 0) = \mu_1(\varphi_1(x_1)) - D_1 = 0.$$

From (2.2) and (2.3), we have

$$\varphi_1(x_1) = \lambda_1 = S_{in} - \frac{D_1}{D}\tilde{x}_1, \quad \text{i.e.} \quad \tilde{x}_1 = \frac{D}{D_1}(S_{in} - \lambda_1).$$

In addition, from Proposition 2.6 and system (2.8), we obtain

$$\bar{x}_1 = F_2(0), \quad \text{i.e.} \quad f_2(0, \bar{x}_1) = \mu_2(S_{in} - g(\bar{x}_1, 0)) - D_2 = 0,$$

that is, $S_{in} - g(\bar{x}_1, 0) = \lambda_2$. Using (2.7), it follows that

$$\bar{x}_1 = \frac{D}{D_1}(S_{in} - \lambda_2).$$

Consequently, $\bar{x}_1 < \tilde{x}_1$ is equivalent to $\lambda_1(D) < \lambda_2(D)$. Similarly, $\mathcal{E}_2$ is LES if and only if $\bar{x}_2 < \tilde{x}_2$ which is equivalent to $\lambda_2(D) < \lambda_1(D)$ where

$$\tilde{x}_2 = \frac{D}{D_2}(S_{in} - \lambda_2) \quad \text{and} \quad \bar{x}_2 = \frac{D}{D_2}(S_{in} - \lambda_1).$$

Recall from Table 2 that the positive steady state $\mathcal{E}^*$ is LES if and only if $F_1'(x_1^*)\,F_2'(x_2^*) > 1$ (or equivalently $c_3(S_{in}, D) > 0$) and $c_4(S_{in}, D) > 0$. Since $Q_{21} = Q_{22} = 0$ and $S^* = \lambda_2$ in the particular case where the function $q_2(x_2, x_1) = 0$, some coefficients of the Jacobian matrix J^* defined in (3.1) change and we obtain $m_{32} = m_{33} = 0$ and $m_{13} = D_2$. From (3.2), it follows that

$$c_3 = m_{13}m_{22}m_{31} - m_{12}m_{23}m_{31}.$$

Using (2.11) and (3.1), we get

$$c_3 = \alpha_1 E_2 \mu_1(\lambda_2) x_1 x_2^3 \left(\frac{D_2}{\mu_1(\lambda_2)} - 2\frac{x_1}{x_2} \right).$$

Since we have $\delta'(x_2) = -c^+ = -D_2/\mu_1(\lambda_2)$, $H'(x_2) = -2a^+ x_2^{-3}$ and $x_1 = H(x_2) = a^+ x_2^{-2}$, it follows that

$$H'(x_2) = -2\frac{x_1}{x_2}.$$

Therefore,

$$c_3 = \alpha_1 E_2 \mu_1(\lambda_2) x_1 x_2^3 \left(H'(x_2) - \delta'(x_2) \right).$$

On the other hand, from (3.6), we see in the particular case where $Q_{22} = Q_{21} = 0$ that $c_4 > 0$. Consequently, $\mathcal{E}^*$ is LES if and only if $H'(x_2^*) > \delta'(x_2^*)$. Now, we can state the following result.

Table 8

Necessary and sufficient conditions of existence and stability of all steady states of model (6.1).

Steady state	Existence	Local stability
$\mathcal{E}_0 = (S_{in}, 0, 0)$	always exists	$S_{in} < \min(\lambda_1(D), \lambda_2(D))$
$\mathcal{E}_1 = (\lambda_1, D(S_{in} - \lambda_1)/D_1, 0)$	$S_{in} > \lambda_1(D)$	$\lambda_1(D) < \lambda_2(D)$
$\mathcal{E}_2 = (\lambda_2, 0, D(S_{in} - \lambda_2)/D_2)$	$S_{in} > \lambda_2(D)$	$\lambda_2(D) < \lambda_1(D)$
$\mathcal{E}_1^* = (\lambda_2, x_1^*, x_2^*)$	$\lambda_1(D) < \lambda_2(D)$, $S_{in} > S_{in}^c$	LES whenever it exists
$\mathcal{E}_2^* = (\lambda_2, x_1^{**}, x_2^{**})$	$\lambda_1(D) < \lambda_2(D)$, $S_{in} > S_{in}^c$	Always unstable

Proposition 6.1. *Assume that Hypothesis 2.1 holds. System (6.1) has at most two positive steady states denoted by $\mathcal{E}_1^* = (\lambda_2, x_1^*, x_2^*)$ and $\mathcal{E}_2^* = (\lambda_2, x_1^{**}, x_2^{**})$ such that $x_1^* < x_1^{**}$. The components (x_1^*, x_2^*) and (x_1^{**}, x_2^{**}) are given by the intersection of the curve of the function $H(x_2)$ defined in (6.5) and the straight line Δ defined in (6.6) by the equation $x_1 = \delta(x_2)$ (see Figure 7). The necessary and sufficient conditions of existence and local stability of all steady states of model (6.1) are given in Table 8.*

In [30], the author could not demonstrate that in reality the condition $c_4 > 0$ of the Routh–Hurwitz criterion corresponding to the stability of the positive steady state $\mathcal{E}_1^*$ of their model (6.1) is always satisfied. Here, we have demonstrate that c_4 is always positive such that the positive steady state $\mathcal{E}_1^*$ is LES whenever it exists and it cannot be destabilized by a Hopf bifurcation with the emergence of a stable limit cycle.

In what follows, we study theoretically the operating diagram of system (6.1). In Table 9, we define the set $\Upsilon_k = \{\Upsilon_1, \Upsilon_2, \Upsilon_5\}$ of the three curves separating the various regions of the (S_{in}, D)-plane.

Table 9

The curves in the set Υ_k and their corresponding colors in Figure 8.

Υ_k	Color
$\Upsilon_1 = \{(S_{in}, D) : S_{in} = \lambda_1(D)\}$	Blue
$\Upsilon_2 = \{(S_{in}, D) : S_{in} = \lambda_2(D)\}$	Red
$\Upsilon_5 = \{(S_{in}, D) : S_{in} = S_{in}^c(D)\}$	Green

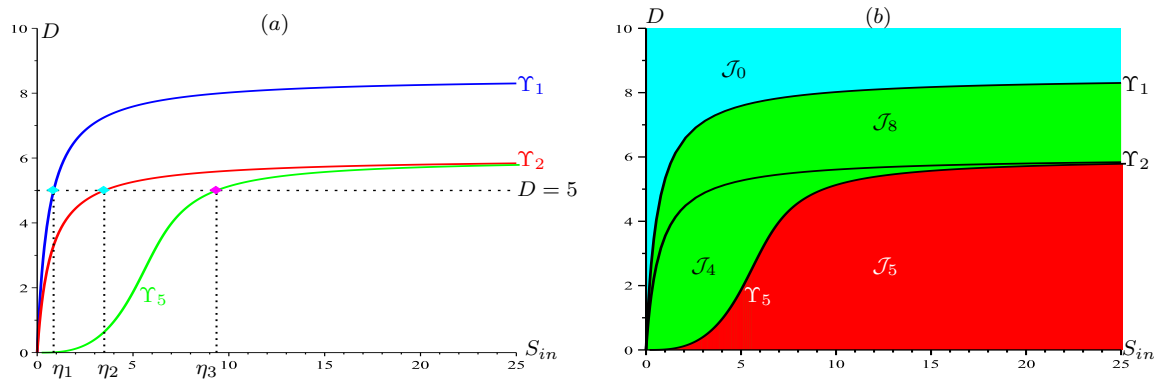

Figure 8. *MAPLE: (a) the three curves Υ_1, Υ_2 and Υ_5 in the (S_{in}, D)-plane. (b) The corresponding operating diagram of model (6.1).*

To illustrate the operating diagram of model (6.1), we choose the specific growth rates (4.2) satisfying Hypothesis 2.1 and the biological parameter values provided in Table 14 which are the same as those in [30]. Since we have the explicit expression of the function $S_{in}^c(D)$ corresponding to the curve Υ_5, MAPLE was able to plot all the curves in the set Υ_k (see Figure 8).

Proposition 6.2. *For the specific growth rates μ_1 and μ_2 defined in (4.2) and the set of the biological parameter values in Table 14, the existence and the local stability of all steady states of (6.1) in the four regions $\mathcal{J}_k$, $k = 0, \ldots, 3$ of the operating diagram in Figure 8 are described in Table 10.*

The following result determines the different types of bifurcations by crossing the four regions $\mathcal{J}_k$, $k = 0, 4, 5, 8$ of the operating diagram in Figure 8.

Proposition 6.3. *The nature of all the bifurcations of steady states of system (6.1) by passing between the various regions of the operating diagram is provided in Table 11.*

Table 10

Existence and local stability of all steady states in the various regions of the operating diagram in Figure 8.

Condition	Region	Color	$\mathcal{E}_0$	$\mathcal{E}_1$	$\mathcal{E}_2$	$\mathcal{E}_1^*$	$\mathcal{E}_2^*$
$S_{in} < \lambda_1(D) < \lambda_2(D)$	$\mathcal{J}_0$	Cyan	S				
$\lambda_1(D) < S_{in} < \lambda_2(D)$	$\mathcal{J}_8$	Green	U	S			
$\lambda_2(D) < S_{in} < S_{in}^c(D)$	$\mathcal{J}_4$	Green	U	S	U		
$S_{in}^c(D) < S_{in}$	$\mathcal{J}_5$	Red	U	S	U	S	U

Table 11

Nature of all the bifurcations of steady states of model (6.1) by crossing the curves Υ_1, Υ_2 and Υ_5.

Transition	Curve	Bifurcation	Steady states
$\mathcal{J}_0$ to $\mathcal{J}_8$	Υ_1	BP	$\mathcal{E}_0 = \mathcal{E}_1$
$\mathcal{J}_8$ to $\mathcal{J}_4$	Υ_2	BP	$\mathcal{E}_0 = \mathcal{E}_2$
$\mathcal{J}_4$ to $\mathcal{J}_5$	Υ_5	LP	$\mathcal{E}_1^* = \mathcal{E}_2^*$

Next, we will show the nature of bifurcations by crossing the different regions of the operating diagram through the three curves Υ_1, Υ_2 and Υ_5. To this end, we will analyze the one-parameter bifurcation diagram in S_{in} where the dilution rate is fixed at $D = 5$. This diagram corresponds to a horizontal line of equation $D = 5$ in the operating diagram (see Figure 8(a)). Figure 9 illustrates in MAPLE the one-parameter bifurcation diagram in S_{in}, with S, x_1 and x_2 on the y-axis.

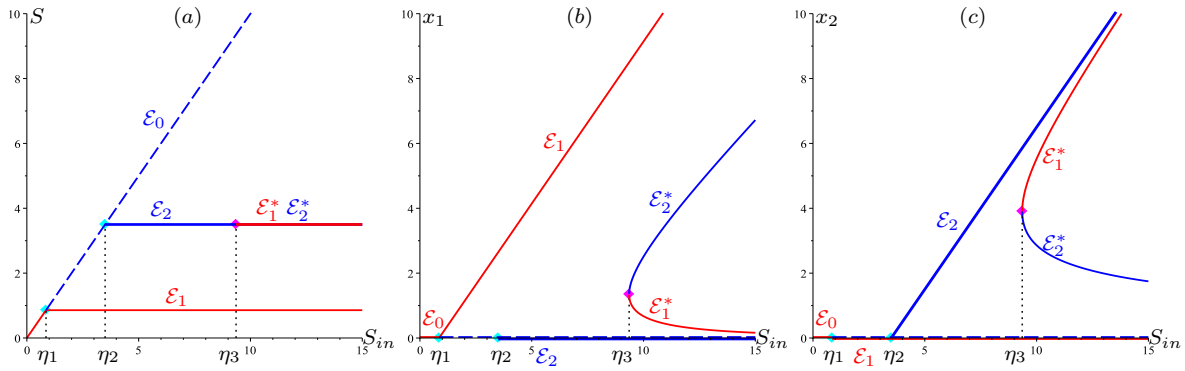

Figure 9. *MAPLE: (a-b-c) one-parameter bifurcation diagrams of system (6.1) in the variables S, x_1, x_2, (resp.), with S_{in} as the bifurcation parameter and $D = 5$.*

Increasing S_{in} from zero, there is a BP bifurcation occurring at $S_{in} = \eta_1 \approx 0.857$ between $\mathcal{E}_0$ and $\mathcal{E}_1$. Indeed, the washout steady state $\mathcal{E}_0$ becomes unstable while the steady state of exclusion of the second species $\mathcal{E}_1$ emerges stable into the admissible region. Next, there is a BP bifurcation at $S_{in} = \eta_2 \approx 3.5$ between the washout steady state $\mathcal{E}_0$ and the steady state of exclusion of the first species $\mathcal{E}_2$ such that $\mathcal{E}_0$ remains unstable and $\mathcal{E}_2$ appears unstable. Finally, an LP bifurcation occurs at $S_{in} = \eta_3 \approx 9.357$ that gives birth to stable and unstable coexistence steady states $\mathcal{E}_1^*$ and $\mathcal{E}_2^*$, respectively. The study of the one-parameter bifurcation diagram in S_{in} from the operating diagram in Figure 8 is summarized in the following result.

Proposition 6.4. *For the specific growth rates μ_1 and μ_2 defined in (4.2) and the set of the biological parameter values in Table 14 corresponding to the operating diagram in Figure 8, the existence and the local stability of all steady states of (6.1) according to S_{in} are described in Table 12 when $D = 5$ is fixed. The critical values η_1, η_2 and η_3 of different bifurcations and the corresponding nature of bifurcations are determined in Table 13.*

Table 12

Existence and stability of steady states of model (6.1) according to S_{in} when $D = 5$. η_1, η_2 and η_3 are defined in Table 13.

Interval of S_{in}	$\mathcal{E}_0$	$\mathcal{E}_1$	$\mathcal{E}_2$	$\mathcal{E}_1^*$	$\mathcal{E}_2^*$
$(0, \eta_1)$	S				
(η_1, η_2)	U	S			
(η_2, η_3)	U	S	U		
$(\eta_3, +\infty)$	U	S	U	S	U

Table 13

Definitions of the critical values η_1, η_2 and η_3 of S_{in} and the corresponding nature of bifurcations when $D = 5$ is fixed and $S_{in}^c(D)$ is defined in (6.7).

Definition	Value	Bifurcation
$\eta_1 = \lambda_1(D)$	0.857	BP
$\eta_2 = \lambda_2(D)$	3.5	BP
$\eta_3 = S_{in}^c(D)$	9.357	LP

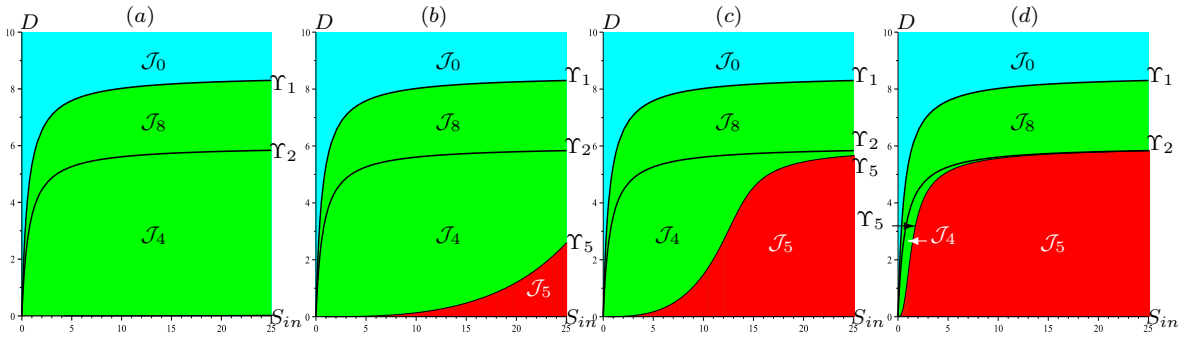

Figure 10. *MAPLE: effect of the variation of the parameter α_1 on the emergence of the coexistence region with bistability in the operating diagram of (6.1): (a) $\alpha_1 = 10^{-5}$, (b) $\alpha_1 = 10^{-3}$ (c) $\alpha_1 = 10^{-2}$, (d) $\alpha_1 = 20$.*

Figure 10 shows the effect of allelopathic interactions of the second species on the first one where there is emergence of the bistability region $\mathcal{J}_5$ (in red) with either coexistence or exclusion of the second species. More precisely, for small enough values of α_1, the operating diagram of the classical chemostat competition model is found where it exhibits the CEP such that only the species with the lowest break-even concentration survives (see Figure 10(a)). Increasing α_1, Figure 10(b-c-d) illustrates how the bistability region $\mathcal{J}_5$ appears and extends while the exclusion regions of the second species are reduced.

Using SCILAB [49], Figure 11(a) illustrates the three-dimensional space (S, x_1, x_2) in the case $S_{in} = 8 < S_{in}^c \approx 9.357$ where there is no interior steady state in $\mathbb{R}^3_+$. For various positive initial conditions even close enough to $\mathcal{E}_0$ or $\mathcal{E}_2$, the numerical simulations permit to conjecture

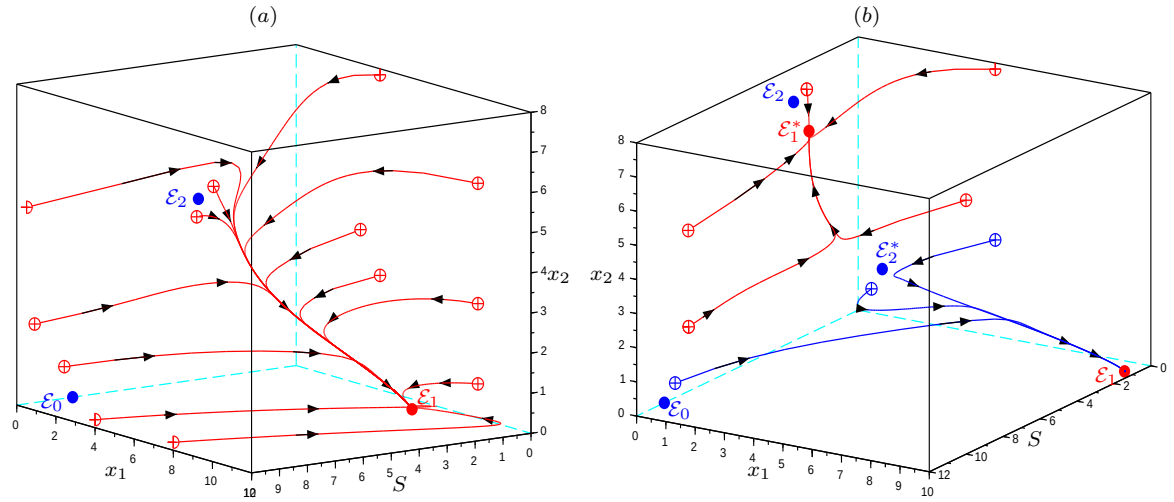

Figure 11. *SCILAB: the three-dimensional space* (S, x_1, x_2) *of* (6.1) *when* $D = 5$*: (a)* $S_{in} = 8 < S_{in}^c \approx 9.357$*, convergence to* $\mathcal{E}_1$*. (b)* $S_{in} = 10.5 > S_{in}^c$*, bistability with either convergence to* $\mathcal{E}_1$ *or* $\mathcal{E}_1^*$*.*

the global convergence towards $\mathcal{E}_1$. In this case, the three steady states are given by

$$\mathcal{E}_0 = (8, 0, 0), \quad \mathcal{E}_1 \simeq (0.857, 7.143, 0) \quad \text{and} \quad \mathcal{E}_2 = (3.5, 0, 4.5).$$

Figure 11(b) shows that system (6.1) exhibits bistability between the steady states $\mathcal{E}_1^*$ of coexistence and $\mathcal{E}_1$ corresponding to the exclusion of second species, when $S_{in} = 10.5 > S_{in}^c$. In this case, there exist five steady states given by $\mathcal{E}_0 = (10.5, 0, 0)$, $\mathcal{E}_1 \simeq (0.857, 9.643, 0)$,

$$\mathcal{E}_2 = (3.5, 0, 7), \ \mathcal{E}_1^* \simeq (3.5, 0.528, 6.234) \text{ and } \mathcal{E}_2^* \simeq (3.5, 3.031, 2.601).$$

Remark 6.5. In the case $\lambda_1 < \lambda_2$, by increasing S_{in}, $\mathcal{E}_1$ loses a degree of stability and $\mathcal{E}_2$ appears locally asymptotically stable for (6.1) is incorrect in Section 2.5 of [30] via a transcritical bifurcation of $\mathcal{E}_0$ and $\mathcal{E}_2$ occurring at $S_{in} = \lambda_2$. Similarly, it is an error in the reverse case $\lambda_2 < \lambda_1$. Indeed, the bifurcation parameter is S_{in} with D is fixed. By Proposition Proposition 6.1, $\mathcal{E}_1$ is LES if and only if $\lambda_1(D) < \lambda_2(D)$. As this last inequality is unchanged by varying S_{in}, then $\mathcal{E}_1$ does not lose a degree of stability and it remains LES (see Figure 9) through the passage of S_{in} by $\lambda_2(D)$ which is fixed. Moreover, $\mathcal{E}_2$ appears unstable via a transcritical bifurcation with $\mathcal{E}_0$ occurring at $S_{in} = \lambda_2$ because $\mathcal{E}_2$ is LES if and only if $\lambda_2(D) < \lambda_1(D)$. Using the same set of parameter values in [30], the numerical simulations in Figure 11(a) illustrating the trajectories in the three-dimensional phase space (S, x_1, x_2) show these contradictions where the solutions of system (6.1) converge to $\mathcal{E}_1$ for any initial condition, in particular for two initial conditions close enough to $\mathcal{E}_2$.

7. Discussion and conclusion. Inspired by the way in which the phenomena of intra- and interspecific interference and allelopathic effects have been formalized to model the competitions of microbial species in [30, 39, 45, 52], we have proposed the original and general model (1.2) of two-microbial species in competition for a single-resource in the chemostat.

Indeed, we have included general intra- and interspecific density-dependent growth rates with allelopathic effects describing the production of each species a toxin that affects the growth of other species as well as its own growth (autotoxicity). The removal rates are distinct so that the mortality rate of each species is the sum of the specific death rate and the autotoxicity. Allowing a large class of growth functions, this model generalized those in [30, 45, 52].

Our mathematical analysis provided a complete study of this process. More precisely, we have determined the necessary and sufficient conditions of existence and local stability of all steady states of model (1.2) according to the operating parameters S_{in} and D. To have a global vision of the asymptotic behavior of model (1.2) according to the operating parameters, we have analyzed theoretically and numerically the operating diagrams in the two parameters S_{in} and D. In fact, we have shown that system (1.2) can have a unique stable steady state: either the washout of two species ($\mathcal{J}_0$), or the exclusion of one species ($\mathcal{J}_1, \mathcal{J}_2$, and $\mathcal{J}_4$), or the coexistence ($\mathcal{J}_3$). The model (1.2) can also exhibit bistability between the coexistence steady state and that of exclusion of the second [resp. first] species ($\mathcal{J}_5$ [resp. $\mathcal{J}_7$]), or the two coexistence steady states ($\mathcal{J}_6$). Crossing the boundary of the various regions in the operating parameters space of model (1.2), we have shown that the steady states can appear or disappear only through transcritical or saddle-node bifurcations. When the input concentration S_{in} is fixed, the analysis of the one-parameter bifurcation diagram in the dilution rate D illustrated the nature of bifurcations of the steady states.

On the other hand, our theoretical results are applied to the particular model (6.1) of Kengwoung-Keumo [30] where the intra- and interspecific interference are neglected, and only the allelopathic effects of the second species on the first species are considered. The necessary and sufficient conditions of existence and local stability of all steady states are established according to the operating parameters S_{in} and D. System (6.1) has at most two coexistence steady states. We have demonstrated that the stability condition of the coexistence steady state $\mathcal{E}_1^*$ in [30] is always fulfilled. Thus, the stability condition of this steady state in [30] must be removed and corrected by the coexistence steady state $\mathcal{E}_1^*$ is LES when it exists.

In addition, we have established theoretically the operating diagram of model (6.1) and we have analyzed the effect of increased toxin production of the second species on the first species. Increasing this allelopathic effect, that is, the value of α_1, the bistability region $\mathcal{J}_5$ (in red) between a coexistence steady state and that of the exclusion of the second species has emerged while the regions of competitive exclusion $\mathcal{J}_4$ and $\mathcal{J}_8$ (in green) are reduced. Decreasing the value of α_1 to zero, we have obtained the operating diagram of the classical chemostat competition model confirming the CEP [27, 50]. The one-parameter bifurcation diagram in S_{in} has described the nature of bifurcations of all steady states by crossing the various regions of the operating diagram in Figure 8 when D is fixed. The numerical simulations have illustrated in the three-dimensional phase space (S, x_1, x_2) either the global convergence towards the steady state of exclusion of the second species or that of the bistability between the coexistence of the two species and the exclusion of second species.

Thus, the main contribution of our study is to bring out the joint effects of the intra- and interspecific competition with the allelopathic effects on the growth of the two species which are not studied in the existing literature. Adding the allelopathic effects of each toxin-producing species to the intra- and interspecific interference of the two species did not allow to solve the open problem of the stability condition c_4 of the Routh–Hurwitz criterion (3.3)

and to show that the coexistence steady state could destabilize with emergence of periodic oscillations. Despite the structure of our model (1.2) being different from that in Fekih-Salem et al. [16], we have found qualitatively similar results for the existence, multiplicity and local stability of the steady states of the two systems. For example, the condition $Q_{11}Q_{22} \geq Q_{12}Q_{21}$ given in Proposition 3.3 is qualitatively similar to condition (26) in [16] which means that the intraspecific interference is dominant with respect to interspecific interference.

In the density-dependence model [16], mortality is essential for there to be any hope of coexistence around periodic oscillations. However, our theoretical study of model (1.2) showed that mortality is not necessary where the coexistence steady state could destabilize even with identical removal rates of the two species. The production effect of a toxic substance released by a species and being nocive to their own or their competitor's growth rates could replace the mortality effect and hope for coexistence around a stable limit cycle.

The application of our general results to the particular model of [30] with only allelopathic effects has shown that there can be coexistence around an interior steady state but in the case where the system exhibits bistability. Thus, the addition of the toxic effect on the most competitive species in the classic chemostat model is sufficient to guarantee the coexistence between the two species but under the constraint of suitable choices of the initial conditions in the basin of attraction of the interior steady state. Moreover, our study also has shown that it is impossible to have coexistence if the second species is more efficient ($\lambda_2 < \lambda_1$) without any effect of intra- and interspecific interference and production of the harmful toxin by the first species in the dynamics of the second species.

Appendix A. Positivity of the stability condition c_4. In this section, we show that the stability condition $c_4 > 0$ holds for the two positive steady states $\mathcal{E}_1^*$ and $\mathcal{E}_3^*$ such that the curve corresponding to $c_4 = 0$ does not exist in the operating diagram of Figure 5 for model (1.2). To this end, we consider the specific growth rates μ_1 and μ_2 defined in (4.2), the functions q_1 and q_2 defined in (4.3), and the set of the biological parameter values in Table 14. Note that the critical values σ_i, $i = 1, \ldots, 6$ of D are defined in Table 7 where σ_i, $i = 1, 2, 3, 6$ correspond to Branch Points (BP) bifurcations while σ_4 and σ_5 correspond to Limit Points (LP) bifurcations. Using MAPLE, we plot in Figure 12(a) the curve of the function $D \mapsto c_4(D)$ corresponding to the steady state $\mathcal{E}_1^*$ [resp. $\mathcal{E}_3^*$] for all D in their existence domain (σ_3, σ_5) [resp. (σ_4, σ_6)] when $S_{in} = 1.4$ and $S_{in} = 2.04$, and in (σ_4, σ_3) [resp. (σ_6, σ_5)] when $S_{in} = 4$, $S_{in} = 8$, and $S_{in} = 16$. Figure 12(b) illustrates a magnification when $D \in [0, 0.2]$ showing the positivity of the function $c_4(D)$ corresponding to the steady state $\mathcal{E}_1^*$ for all $D \in (\sigma_1, \sigma_2)$ and for the different fixed values of S_{in}. Moreover, the numerical simulations show that c_4 is always positive for any value of S_{in} and D in the existence domain of $\mathcal{E}_1^*$ and $\mathcal{E}_3^*$.

Appendix B. Parameter values for numerical simulations. All the values of the parameters used in the numerical simulations are provided in Table 14.

Table 14

Parameter values used for models (1.2) and (6.1) when the growth rates μ_1 and μ_2 are given by (4.2) and the functions q_1 and q_2 are defined in (4.3).

Parameter	μ_1^m	k_1	μ_2^m	k_2	a_{11}	a_{12}	α_1	a_{22}	a_{21}	α_2	θ_1	m_1	θ_2	m_2
Figures 4 to 6 and 12	7.5	0.5	8.5	1.2	5	6	22	7	5	22	0.8	0.7	0.1	0.1
Figures 7 to 11	8.5	0.6	6	0.7	0	0	0.11	0	0	0	1	0	1	0

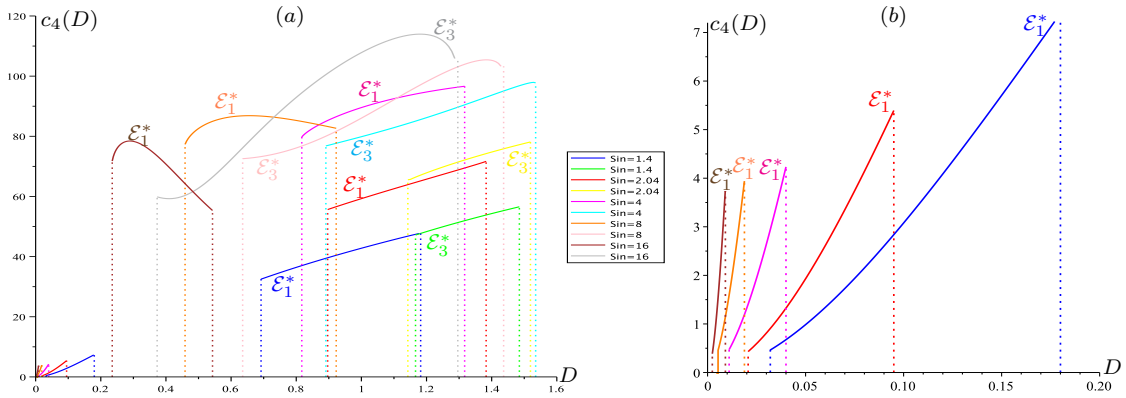

Figure 12. *MAPLE: (a) curves of the function $c_4(D)$ corresponding to $\mathcal{E}_1^*$ [resp. $\mathcal{E}_3^*$] for all D in their existence domain (σ_3, σ_5) [resp. (σ_4, σ_6)] when $S_{in} = 1.4$ and $S_{in} = 2.04$, and in (σ_4, σ_3) [resp. (σ_6, σ_5)] when $S_{in} = 4$, $S_{in} = 8$, and $S_{in} = 16$. (b) Magnification of $c_4(D)$ corresponding to $\mathcal{E}_1^*$ for all $D \in (\sigma_1, \sigma_2)$.*

REFERENCES

[1] N. Abdellatif, R. Fekih-Salem, and T. Sari, *Competition for a single resource and coexistence of several species in the chemostat*, Math. Biosci. Eng., 13 (2016), pp. 631–652, https://doi.org/10.3934/mbe.2016012.

[2] M. Ballyk, R. Staffeldt, and I. Jawarneh, *A nutrient-prey-predator model: Stability and bifurcations*, Discrete and Continuous Dyn. Syst. - S, 13 (2020), pp. 2975–3004, https://doi.org/10.3934/dcdss.2020192.

[3] B. Bar and T. Sari, *The operating diagram for a model of competition in a chemostat with an external lethal inhibitor*, Discrete and Continuous Dyn. Syst. - B, 25 (2020), pp. 2093–2120, https://doi.org/10.3934/dcdsb.2019203.

[4] O. Bernard, Z. Hadj-Sadok, D. Dochain, A. Genovesi, and J.-P. Steyer, *Dynamical model development and parameter identification for an anaerobic wastewater treatment process*, Biotechnol. Bioeng., 75 (2001), pp. 424–438, https://doi.org/10.1002/bit.10036.

[5] M. P. Boer, B. W. Kooi, and S. A. L. M. Kooijman, *Food chain dynamics in the chemostat*, Math. Biosci., 150 (1998), pp. 43–62, https://doi.org/10.1016/S0025-5564(98)00010-8.

[6] G. J. Butler and G. S. K. Wolkowicz, *Predator-mediated competition in the chemostat*, J. Math. Biol., 24 (1986), pp. 167–191, https://doi.org/10.1007/BF00275997.

[7] J. Chattopadhyay, *Effect of toxic substances on a two-species competitive system*, Ecol. Modell., 84 (1996), pp. 287–289, https://doi.org/10.1016/0304-3800(94)00134-0.

[8] Y. Daoud, N. Abdellatif, T. Sari, and J. Harmand, *Steady state analysis of a syntrophic model: The effect of a new input substrate concentration*, Math. Model. Nat. Phenom., 13 (2018), pp. 1–22, https://doi.org/10.1051/mmnp/2018037.

[9] P. De Leenheer, D. Angeli, and E. D. Sontag, *Crowding effects promote coexistence in the chemostat*, J. Math. Anal. Appl., 319 (2006), pp. 48–60, https://doi.org/10.1016/j.jmaa.2006.02.036.

[10] M. Dellal and B. Bar, *Global analysis of a model of competition in the chemostat with internal inhibitor*, Discrete and Continuous Dyn. Syst. - B, 26 (2021), pp. 1129–1148, https://doi.org/10.3934/dcdsb.2020156.

[11] M. Dellal, B. Bar, and M. Lakrib, *A competition model in the chemostat with allelopathy and substrate inhibition*, Discrete and Continuous Dyn. Syst. - B, 27 (2022), pp. 2025–2050, https://doi.org/10.3934/dcdsb.2021120.

[12] M. Dellal, M. Lakrib, and T. Sari, *The operating diagram of a model of two competitors in a chemostat with an external inhibitor*, Math. Biosci., 302 (2018), pp. 27–45, https://doi.org/10.1016/j.mbs.2018.05.004.

[13] A. Dhooge, W. Govaerts, Y. A. Kuznetsov, H. G. E. Meijer, and B. Sautois, *New features of the software matcont for bifurcation analysis of dynamical systems*, Math. Comput. Model. Dyn., 14 (2008), pp. 147–175, https://doi.org/10.1080/13873950701742754.

[14] R. Fekih-Salem, Y. Daoud, N. Abdellatifi, and T. Sari, *A mathematical model of anaerobic digestion with syntrophic relationship, substrate inhibition and distinct removal rates*, SIAM J. Appl. Dyn. Syst., 20 (2021), pp. 1621–1654, https://doi.org/10.1137/20M1376480.

[15] R. Fekih-Salem, J. Harmand, C. Lobry, A. Rapaport, and T. Sari, *Extensions of the chemostat model with flocculation*, J. Math. Anal. Appl., 397 (2013), pp. 292–306, https://doi.org/10.1016/j.jmaa.2012.07.055.

[16] R. Fekih-Salem, C. Lobry, and T. Sari, *A density-dependent model of competition for one resource in the chemostat*, Math. Biosci., 286 (2017), pp. 104–122, https://doi.org/10.1016/j.mbs.2017.02.007.

[17] R. Fekih-Salem, A. Rapaport, and T. Sari, *Emergence of coexistence and limit cycles in the chemostat model with flocculation for a general class of functional responses*, Appl. Math. Modell., 40 (2016), pp. 7656–7677, https://doi.org/10.1016/j.apm.2016.03.028.

[18] R. Fekih-Salem and T. Sari, *Properties of the chemostat model with aggregated biomass and distinct removal rates*, SIAM J. Appl. Dyn. Syst. (SIADS), 18 (2019), pp. 481–509, https://doi.org/10.1137/18M1171801.

[19] R. Fekih-Salem and T. Sari, *Operating diagram of a flocculation model in the chemostat*, ARIMA J., 31 (2020), pp. 45–58, https://hal.archives-ouvertes.fr/hal-02160798.

[20] R. Fekih-Salem, T. Sari, and N. Abdellatif, *Sur un modèle de compétition et de coexistence dans le chémostat*, ARIMA J., 14 (2011), pp. 15–30, http://arima.inria.fr/014/014002.html.

[21] P. Fergola, M. Cerasuolo, A. Pollio, G. Pinto, and M. DellaGreca, *Allelopathy and competition between chlorella vulgaris and pseudokirchneriella subcapitata: Experiments and mathematical model*, Ecol. Modell., 208 (2007), pp. 205–214, https://doi.org/https://doi.org/10.1016/j.ecolmodel.2007.05.024.

[22] P. Fergola, J. Li, and Z. Ma, *On the dynamical behavior of some algal allelopathic competitions in chemostat-like environment.*, Ricerche mat., 60 (2011), pp. 313–332, https://doi.org/https://doi.org/10.1007/s11587-011-0108-y.

[23] J. Grover, *Resource Competition*, vol. 1, Springer New York, NY, 1997, https://doi.org/10.1007/978-1-4615-6397-6.

[24] B. Haegeman and A. Rapaport, *How flocculation can explain coexistence in the chemostat*, J. Biol. Dyn., 2 (2008), pp. 1–13, https://doi.org/10.1080/17513750801942537.

[25] M. Hanaki, J. Harmand, Z. Mghazli, A. Rapaport, T. Sari, and P. Ugalde, *Mathematical study of a two-stage anaerobic model when the hydrolysis is the limiting step*, Processes, 9 (2021), p. 2050, https://doi.org/10.3390/pr9112050.

[26] S. R. Hansen and S. P. Hubbell, *Single-nutrient microbial competition: Qualitative agreement between experimental and theoretically forecast outcomes*, Science, 207 (1980), pp. 1491–1493.

[27] J. Harmand, C. Lobry, A. Rapaport, and T. Sari, *The Chemostat: Mathematical Theory of Microorganism Cultures*, vol. 1, Chemical Eng. Ser., Chemostat Bioprocesses Set, Wiley, New York, 2017, https://doi.org/10.1002/9781119437215.

[28] S. B. Hsu, C. A. Klausmeier, and C. J. Lin, *Analysis of a model of two parallel food chains*, Discrete and Continuous Dyn. Syst. - B, 12 (2009), pp. 337–359, https://doi.org/10.3934/dcdsb.2009.12.337.

[29] S. B. Hsu and P. Waltman, *Competition in the chemostat when one competitor produces a toxin*, Japan J. Indust. Appl. Math., 15 (1998), pp. 471–490, https://doi.org/10.1007/BF03167323.

[30] J.-J. Kengwoung-Keumo, *Competition between a nonallelopathic phytoplankton and an allelopathic phytoplankton species under predation*, Math. Biosci. Eng., 13 (2016), pp. 787–812, https://doi.org/10.3934/mbe.2016018.

[31] Z. Khedim, B. Benyahia, B. Cherki, T. Sari, and J. Harmand, *Effect of control parameters on biogas production during the anaerobic digestion of protein-rich substrates*, Appl. Math. Model., 61 (2018), pp. 351–376, https://doi.org/10.1016/j.apm.2018.04.020.

[32] B. Li and Y. Kuang, *Simple food chain in a chemostat with distinct removal rates*, J. Math. Anal. Appl., 242 (2000), pp. 75–92, https://doi.org/10.1006/jmaa.1999.6655.

[33] C. Lobry and J. Harmand, *A new hypothesis to explain the coexistence of n species in the presence of a single resource*, C. R. Biol., 329 (2006), pp. 40–46, https://doi.org/10.1016/j.crvi.2005.10.004.

[34] C. Lobry, F. Mazenc, and A. Rapaport, *Persistence in ecological models of competition for a single resource*, C. R. Acad. Sci. Paris Ser. I, 340 (2005), pp. 199–204, https://doi.org/10.1016/j.crma.2004.12.021.

[35] C. Lobry, A. Rapaport, and F. Mazenc, *Sur un modèle densité-dépendant de compétition pour une ressource*, C. R. Biol., 329 (2006), pp. 63–70, https://doi.org/10.1016/j.crvi.2005.11.004.

[36] MAPLE [Software], Waterloo Maple Inc., *Waterloo, Ontario*, https://fr.maplesoft.com/.
[37] I. P. Martines, H. V. Kojouharov, and J. P. Grover, *A chemostat model of resource competition and allelopathy*, Appl. Math. Comput., 215 (2009), pp. 573–582, https://doi.org/10.1016/j.amc.2009.05.033.
[38] MATCONT [Software], W. Govaerts, Y. A. Kuznetsov, and H.G.E. Meijer, https://sourceforge.net/projects/matcont/.
[39] J. Maynard-Smith, *Models in Ecology*, Cambridge University Press, London, 1974.
[40] T. Mtar, R. Fekih-Salem, and T. Sari, *Interspecific density-dependent model of predator-prey relationship in the chemostat*, Int. J. Biomath., 14 (2021), p. 2050086, https://doi.org/10.1142/S1793524520500862.
[41] T. Mtar, R. Fekih-Salem, and T. Sari, *Mortality can produce limit cycles in density-dependent models with a predator-prey relationship*, Discrete and Continuous Dyn. Syst. - B, 27 (2022), pp. 7445–7467, https://doi.org/10.3934/dcdsb.2022049.
[42] S. Nouaoura, N. Abdellatif, R. Fekih-Salem, and T. Sari, *Mathematical analysis of a three-tiered model of anaerobic digestion*, SIAM J. Appl. Math., 81 (2021), pp. 1264–1286, https://doi.org/10.1137/20M1353897.
[43] S. Nouaoura, R. Fekih-Salem, N. Abdellatif, and T. Sari, *Mathematical analysis of a three-tiered food-web in the chemostat*, Discrete and Continuous Dyn. Syst. - B, 26 (2021), pp. 5601–5625, https://doi.org/10.3934/dcdsb.2020369.
[44] S. Nouaoura, R. Fekih-Salem, N. Abdellatif, and T. Sari, *Operating diagrams for a three-tiered microbial food web in the chemostat*, J. Math. Biol., 85 (2022), https://doi.org/10.1007/s00285-022-01812-5.
[45] S. Roy, *The coevolution of two phytoplankton species on a single resource: Allelopathy as a pseudo-mixotrophy*, Theor. Popul. Biol., 75 (2009), pp. 68–75, https://doi.org/https://doi.org/10.1016/j.tpb.2008.11.003.
[46] T. Sari and B. Benyahia, *The operating diagram for a two-step anaerobic digestion model*, Nonlinear Dyn., 105 (2021), pp. 2711–2737, https://doi.org/10.1007/s11071-021-06722-7.
[47] T. Sari and J. Harmand, *A model of a syntrophic relationship between two microbial species in a chemostat including maintenance*, Math. Biosci., 275 (2016), pp. 1–9, https://doi.org/10.1016/j.mbs.2016.02.008.
[48] T. Sari and M. J. Wade, *Generalised approach to modelling a three-tiered microbial food-web*, Math. Biosci., 291 (2017), pp. 21–37, https://doi.org/10.1016/j.mbs.2017.07.005.
[49] SCILAB [Software], *Enterprises SAS*, https://www.scilab.org/.
[50] H. Smith and P. Waltman, *The Theory of the Chemostat: Dynamics of Microbial Competition*, Cambridge University Press, Cambridge, UK, 1995.
[51] S. Sobieszek, M. J. Wade, and G. S. K. Wolkowicz, *Rich dynamics of a three-tiered anaerobic food-web in a chemostat with multiple substrate inflow*, Math. Biosci. Eng., 17 (2020), pp. 7045–7073, https://doi.org/10.3934/mbe.2020363.
[52] J. Solé, E. García-Ladona, P. Ruardij, and M. Estrada, *Modelling allelopathy among marine algae*, Ecological Modelling, 183 (2005), pp. 373–384, https://doi.org/10.1016/j.ecolmodel.2004.08.021.
[53] M. J. Wade, J. Oakley, S. Harbisher, N. G. Parker, and J. Dolfing, *MI-Sim: A MATLAB package for the numerical analysis of microbial ecological interactions*, PLoS ONE., 12 (2017), p. e0173249, https://doi.org/10.1371/journal.pone.0173249.
[54] M. J. Wade, R. W. Pattinson, N. G. Parker, and J. Dolfing, *Emergent behaviour in a chlorophenol-mineralising three-tiered microbial 'food web'*, J. Theor. Biol., 389 (2016), pp. 171–186, https://doi.org/10.1016/j.jtbi.2015.10.032.
[55] M. Weedermann, G. S. K. Wolkowicz, and J. Sasara, *Optimal biogas production in a model for anaerobic digestion*, Nonlinear Dyn, 81 (2015), pp. 1097–1112, https://doi.org/10.1007/s11071-015-2051-z.
[56] G. S. K. Wolkowicz, *Successful invasion of a food web in a chemostat*, Math. Biosci., 93 (1989), pp. 249–268, https://doi.org/10.1016/0025-5564(89)90025-4.
[57] A. Xu, J. Dolfing, T. P. Curtis, G. Montague, and E. Martin, *Maintenance affects the stability of a two-tiered microbial 'food chain'?*, J. Theor. Biol., 276 (2011), pp. 35–41, https://doi.org/10.1016/j.jtbi.2011.01.026.